

The stability of stellar disks in Milky-Way sized dark matter halos

Denis Yurin^{1,2} and Volker Springel^{1,2}

¹Heidelberg Institute for Theoretical Studies, Schloss-Wolfsbrunnengasse 35, 69118 Heidelberg, Germany

²Zentrum für Astronomie der Universität Heidelberg, ARI, Mönchhofstr. 12-14, 69120 Heidelberg, Germany

10 October 2018

ABSTRACT

We employ an improved methodology to insert live stellar disks into high-resolution dark matter simulations of Milky Way sized halos, allowing us to investigate the fate of thin stellar disks in the tumultuous environment of cold dark matter structures. We study a set of eight different halos, drawn from the Aquarius simulation project, in which stellar disks are adiabatically grown with a prescribed structure, and then allowed to self-consistently evolve. The initial velocity distribution is set-up in very good equilibrium with the help of the GALIC code. We find that the residual triaxiality of the halos leads to significant disk tumbling, qualitatively confirming earlier work. We show that the disk turning motion is unaffected by structural properties of the galaxies such as the presence or absence of a bulge or bar. In typical Milky Way sized dark matter halos, we expect an average turning of the disks by about 40 degrees between $z = 1$ and $z = 0$, over the course of 7.6 Gyr. We also investigate the impact of the disks on substructures, and conversely, the disk heating rate caused by the dark matter halo substructures. The presence of disks reduces the central subhalo abundance by a factor of two, due to an increased evaporation rate by gravitational shocks from disk passages. We find that substructures are important for heating the outer parts of stellar disks but do not appear to significantly affect their inner parts.

Key words: methods: numerical – galaxies: formation – galaxies: kinematics and dynamics – cosmology: theory – dark matter.

1 INTRODUCTION

The Λ cold dark matter (Λ CDM) cosmogony represents the leading theoretical model for structure formation and predicts a hierarchical growth of galaxies in which dark matter halos have prominent triaxial shapes (Frenk et al. 1988) and are full of substructures (Moore et al. 1999). It is not well understood how grand design spiral galaxies can form and survive in this violent environment, which seems at the outset quite hostile towards the long-term survival of thin, cold stellar disks. Such disks may easily become distorted and tilted by triaxial potentials, they may suffer from bar instabilities or excessive heating from dark matter substructures and merger events.

Until recently, full hydrodynamical cosmological simulations have not been particularly successful in making realistic thin disk galaxies without dominating bulges, even though some remarkable progress has lately been achieved on this long-standing problem (Heller et al. 2007; Governato et al. 2010; Agertz et al. 2011; Guedes et al. 2011; Aumer et al. 2013; Stinson et al. 2013; Marinacci et al. 2014a). But even in the most recent simulation works, the disks have generally been found to be too thick (e.g. Marinacci et al. 2014a). This could plausibly be related to inaccurate modelling of the disk formation physics, to a lack of numerical resolution, or to a combination thereof. However, another possibil-

ity is that the hierarchical nature of dark matter halo growth in cold dark matter models, combined with the strong triaxiality of CDM halos, quite generally causes excessive disk heating. In this case, CDM scenarios may pose restrictive intrinsic limits on the possible abundance of thin stellar disks. It is therefore important to shed more light on the question under which conditions thin stellar disks can comfortably survive in CDM halos.

It is difficult to study this issue systematically with full cosmological hydrodynamical simulations, due to their very high computational cost and the lack of freedom to prescribe the structural disk properties of the galaxies. An alternative approach is to study the stability of well-resolved collisionless stellar disks that are inserted into dark matter halos in a suitable fashion. This has been explored in numerous previous works, but most of these studies employed isolated toy models of halos and disks, and not the full cosmological context (e.g. Walker et al. 1996; Sellwood et al. 1998; Velazquez & White 1999; Athanassoula 2002; Debattista et al. 2006; Gauthier et al. 2006; Kazantzidis et al. 2008; Read et al. 2008; Machado & Athanassoula 2010). Only a few works have tried to achieve a consistent cosmological embedding, where the disk is somehow inserted by hand in a suitable fashion in a growing dark matter halo. Pioneering work in this direction was done by Berentzen et al. (2006) for isolated halos and by

Series #	Simulation names	Disk parameters		Orientation	Bulge parameters		ϵ_{grav} [kpc]	Notes
		M_d [$10^{10} M_{\odot}$]	N_{disk}		M_b [$10^{10} M_{\odot}$]	N_{bulge}		
1	'A5..H5-minor'	5.0	2×10^5	minor			0.68	
	'A4-minor'	5.0	1.6×10^6	minor			0.34	
	'A3-minor'	5.0	1.28×10^7	minor			0.17	
2	'A5..H5-major'	5.0	2×10^5	major			0.68	
3	'A5..H5-with-bulge-minor'	3.33	2×10^5	minor	1.67	1×10^5	0.68	
	'A4-with-bulge-minor'	3.33	1.6×10^6	minor	1.67	8×10^5	0.34	
	'A3-with-bulge-minor'	3.33	1.28×10^7	minor	1.67	3.2×10^6	0.17	
4	'A5..H5-lighter-disk-minor'	3.33	2×10^5	minor			0.68	
5	'A5..H5-massive-bulge-minor'	1.67	2×10^5	minor	3.33	2×10^5	0.68	
6	'A5..H5-rounded-minor'	5.0	2×10^5	minor			0.68	rounded dark halo (like #1)
7	'A5..H5-withbulge-rounded'	3.33	2×10^5	minor	1.67	1×10^5	0.68	rounded dark halo (like #3)
8	'A5..H5-subst-wiped-minor'	5.0	2×10^5	minor			0.68	rounded dark halo (like #1)
9	'A5..H5-withbulge-subst-wiped'	3.33	2×10^5	minor	1.67	1×10^5	0.68	rounded dark halo (like #3)
10	'A5..H5-reorient-minor'	5.0	2×10^5	minor			0.68	growth phase reorientation
11	'A5..H5-reorient-major'	5.0	2×10^5	major			0.68	growth phase reorientation
12	'A5..H5-late-insert-minor'	5.0	2×10^5	minor			0.68	$z_{\text{ins}} = 0.5, z_{\text{live}} = 0.364$

Table 1. Overview of our simulation sets and their basic numerical parameters. We have organized the runs in different series, as illustrated in the table. The first series consists of our default pure disk runs, inserted along the minor axis. Here we also carried out runs for the A-halo at 8 times and 64 times higher resolution, respectively. Series #2 repeats the level-5 runs with a major orientation of the disk. In series #3 we replace the disk with a bulge+disk system in which one third of the mass is moved to a disk. In series #4 this lighter disk is kept but the bulge is omitted, while in series #5 we swap the masses of disk and bulge so that we end up with a relatively massive bulge and a disk of half the mass of the bulge. The remaining series represent special simulations to test various aspects of our procedures. Series #6 and #7 repeat the runs of series #1 and #3, respectively, but this time the dark matter halo is “rounded” when the disk is inserted, as described in the text. Series #8 and #9 restrict the rounding to particles bound in substructures, so that smooth dark matter halos are produced. In series #10 and #11 we have tested for minor and major orientations whether a continuous reorientation of the disk during the growth phase between $z_{\text{insert}} = 1.0$ and $z_{\text{live}} = 1.3$ helps in reducing disk tumbling. Finally, series #12 delays the disk insertion to much later time, where the dark matter halos have relaxed more and therefore may potentially make it easier for disks to survive unaffected.

Berentzen & Shlosman (2006) in a cosmological context where the “seed” stellar disk was inserted and quasi-adiabatically grown in an assembling dark matter halo. These studies revealed the mutual influence of halo and disk on each other and allowed to gain valuable insights on bar formation in the local Universe. Later D’Onghia et al. (2010) applied a similar approach to study the influence of the disk on dark matter substructures and found that the disk can be responsible for a partial depletion of substructures.

The most sophisticated variant of this approach has recently been presented by DeBuhr et al. (2012), who introduced disks in a subset of the halos studied in the “Aquarius” project (Springel et al. 2008a), which consists of high-resolution simulations of Milky Way-sized halos in a Λ CDM universe. The Aquarius halos have been particularly well studied, with a subset of them also being followed up hydrodynamically (Scannapieco et al. 2009, 2012; Aumer et al. 2013, 2014; Marinacci et al. 2014a,b; Pakmor et al. 2014; Okamoto et al. 2015). The corresponding initial conditions exist at different resolutions and are of high quality, allowing converged results even including the density profiles of individual dark matter subhalos (Springel et al. 2008a).

The study of DeBuhr et al. (2012) has examined halos A, B, C, and D of the original Aquarius set. A general result of their work was that disks in CDM halos of Milky-Way sized halos appear to be rather brittle, and can be expected to substantially change over the course of a few Gyrs. In particular, DeBuhr et al. (2012) have found that their disks tumble substantially, and universally grow bars, unless very light disks are used. A substantial fraction of the initial disk material reached large heights above and below the disk plane, and significant warps in the disks were detected as well.

However, DeBuhr et al. (2012) used a comparatively simple method to initialize the disk velocity distribution function, and only one family of initial galaxy structures was considered. In the

present work we try to improve on this earlier work in several respects, in particular by extending the study to a larger halo sample that encompasses eight Aquarius halos, by using a more sophisticated and flexible method to initialize the initial disk models based on our GALIC code (Yurin & Springel 2014), by including also models with stellar bulges, and by checking the robustness of our results with a convergence study at much higher resolution than used in previous work. We also consider additional lines of analysis, for example by examining the mutual impact of the disk and the substructures on to each other. Substructures may induce heating of the disk, but they may also themselves be depleted through gravitational shocks experienced during disk transition or pericentre passage (D’Onghia et al. 2010).

In this work we are especially interested in the question how universal the disk tumbling phenomenon is, and to what extent it is affected by the initial orientation and structure of the disk galaxy relative to its hosting dark matter halo. We would also like to better understand under which conditions strong bars can be avoided in live dark matter halos, and whether the large number of dark matter substructures poses a significant problem for disk stability.

This work is structured as follows. In Section 2 we review the methodology we apply, while in Section 3 we describe the simulation set we have carried out. Section 4 is then devoted to an analysis of our results for pure disk models, whereas in Section 5 we turn to models that also include a central bulge. In Section 6 we briefly analyze the impact of disks on substructures and vice versa, and in Section 7 we examine the robustness of our results with respect to numerical resolution. Finally, we conclude with a discussion and summary in Section 8.

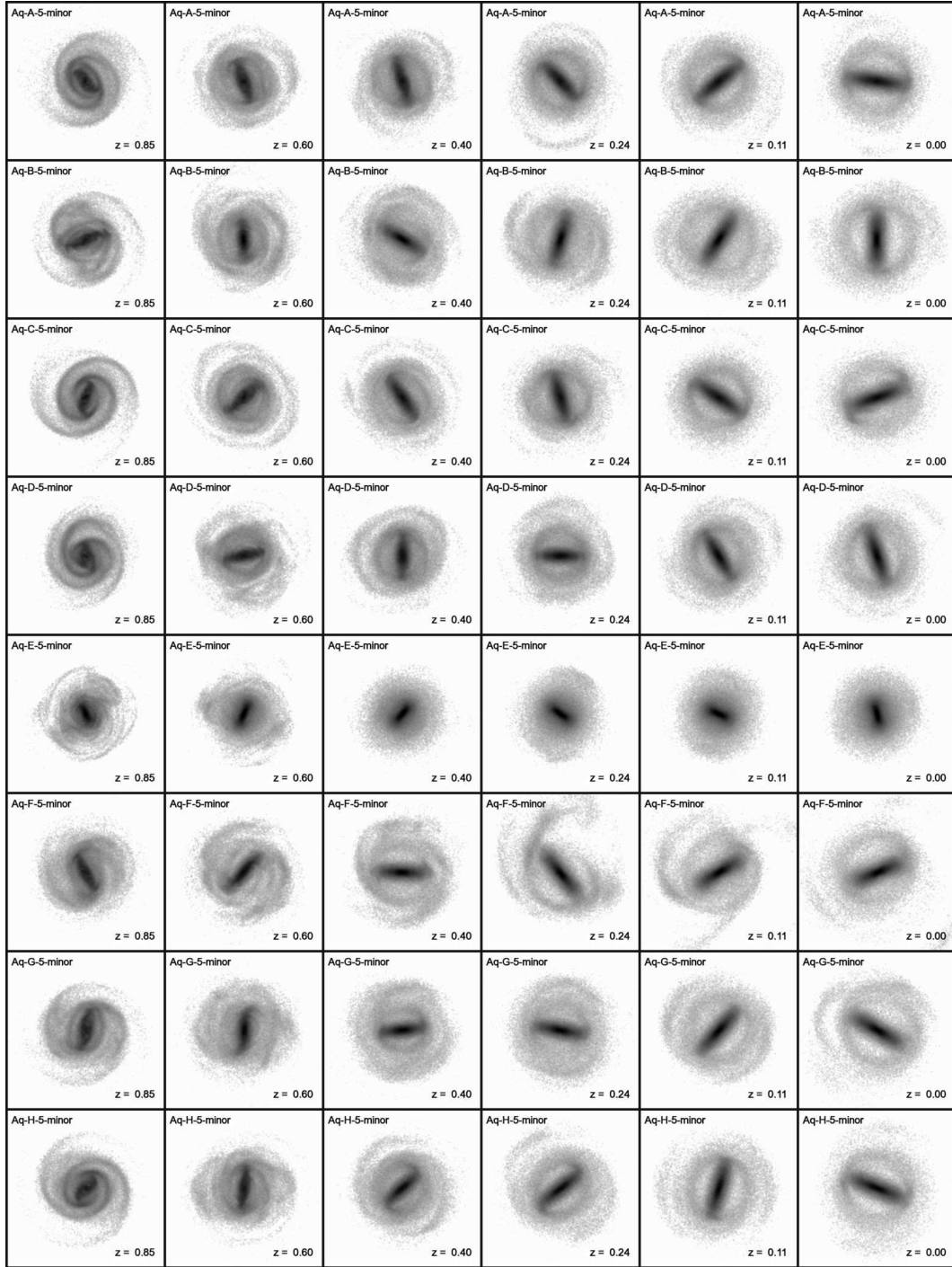


Figure 1. Face-on projections of the stellar mass of the disks in our default runs (series #1). Each row shows a different Aquarius halo, as labelled, with the columns from left to right showing different times ranging from $z = 0.85$ to $z = 0$. Each panel has a fixed physical size of 54 kpc on a side, and uses the same logarithmic grey scale (covering a dynamic range of 1000 in surface density) for visualizing the adaptively smoothed surface density of star particles. In each panel, the stellar particles have been turned independently into a face-on orientation as determined by the angular momentum vector of the stars within the central 5 kpc of the disk.

2 METHODOLOGY

In this study, we carry out resimulations of the “Aquarius” set of initial conditions of Milky Way-sized dark matter halos. They have previously been analyzed in a number of studies (Springel et al. 2008a,b; Navarro et al. 2010; Xu et al. 2009), where in particular the high quality of the zoom initial conditions (created by Adrian

Jenkins) was demonstrated, allowing good convergence of all dark matter properties of the halos. We shall mainly work with resolution ‘level 5’ in the nomenclature of Springel et al. (2008a), where the dark matter halos have close to 1 million particles in the final virial radius, corresponding to a dark matter particle mass of about $\sim 3 \times 10^6 M_{\odot}$. For selected models, we also carry out simula-

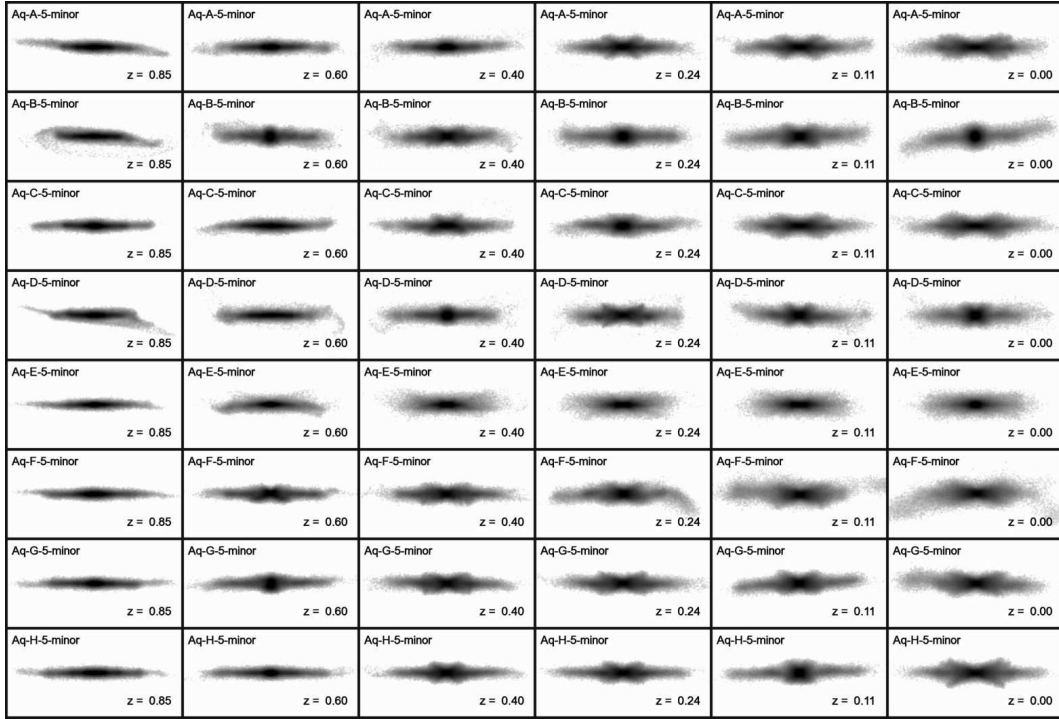


Figure 2. Edge-on projections of the stellar disks in our default runs with pure disks. These images correspond to side-views of the corresponding images shown in Figure 1, with an unchanged physical size of each panel in the horizontal direction (54 kpc), and an identical colour-scale.

tions at 8 times (‘level 4’) and 64 times (‘level 3’) better resolution, reaching up to ~ 50 million particles dark matter and ~ 19 million star particles in the virial radius.

In order to set-up a live stellar disk in the evolving dark matter (re-)simulations of the Aquarius halos, we proceed similarly to DeBuhr et al. (2012). At a certain redshift z_{insert} we place a number N_{disk} of massless star particles into the dark matter halo, sampling a prescribed density distribution placed at the centre of the potential minimum and oriented along one of the principal axes of the halo at that time. The disk mass is then grown linearly in time to a final mass M_d reached at a redshift z_{live} . During the growth phase, the relative distances of the disk particles with respect to each other are kept fixed in physical coordinates, and the whole set of disk particles is coherently moved as a solid body under the total gravitational force experienced by all the particles of the disk. The initial velocity of all the disk particles is set equal to the bulk velocity of the inner dark matter halo (defined as $r < R_{200}/4$, where R_{200} is the radius enclosing a mean overdensity 200 times the critical density). While the disk mass is ramped up, the dark matter particles start to experience the additional gravitational force due to the disk particles, so that the dark matter halo reacts adiabatically to the growing disk. This process of inserting the disk ensures that the disk stays well centred in the moving dark matter halo, and the realization of the disk potential through particles avoids the need to make any approximation in representing the disk potential; in fact, the density structure of the inserted stellar system can be chosen freely as long as it is physical.

When the disk has reached its final mass, we continue the simulation by treating the disk particles as live, which simply means that from this point on they are treated as ordinary collisionless particles with independent orbits in an evolving gravitational potential. This requires an initialization of the initial velocities of the star particles at z_{live} , which should be done such that the disk is in a

self-consistent dynamical equilibrium at this instant. Formally, this corresponds to finding a stationary solution of the Poisson-Vlasov system, which is a quite non-trivial problem for general mass distributions (Binney & Tremaine 1987). In DeBuhr et al. (2012), an approximate solution of the Jeans equation was used to initialize the disk velocities, but the details of this procedure were not described. Here we adopt the method of Yurin & Springel (2014), which iteratively derives a high quality distribution function for the disk particles. The method as implemented in the publicly available GALIC code integrates a large set of test particles representing the target mass distribution in the self-consistent gravitational potential of the system, and adjusts the velocities until the deviation between the time-averaged density response of the particle orbits and the target density distribution is minimized.

In order to take the actual shape of the dark matter halo into account at the moment the disk goes live, we directly use the dark matter particles in the cosmological simulation to compute the halo forces in GALIC. However, as the stable version of the code is at present restricted to axisymmetric disk models, the dark matter halo forces are averaged in the azimuthal direction, i.e. the dark matter force field is ‘axisymmetrized’ without actually changing the dark matter halo. We note that this approximation could be avoided in principle in future refinements of the method, in which case it would then become possible to insert ellipsoidal disks. For the moment, we stick however with inserting axisymmetric disk models with a correspondingly axisymmetric velocity structure. Also, we note that GALIC uses additional constraints on the velocity dispersions in order to single out a desired target solution among the many different degenerate solutions that are in principle possible for reproducing the same density distribution. For example, GALIC can realize disk models with three integrals of motion and tilted velocity ellipsoids, similar to what is observed for the Milky Way (Siebert et al. 2008; Binney et al. 2014; Büdenbender et al. 2014).

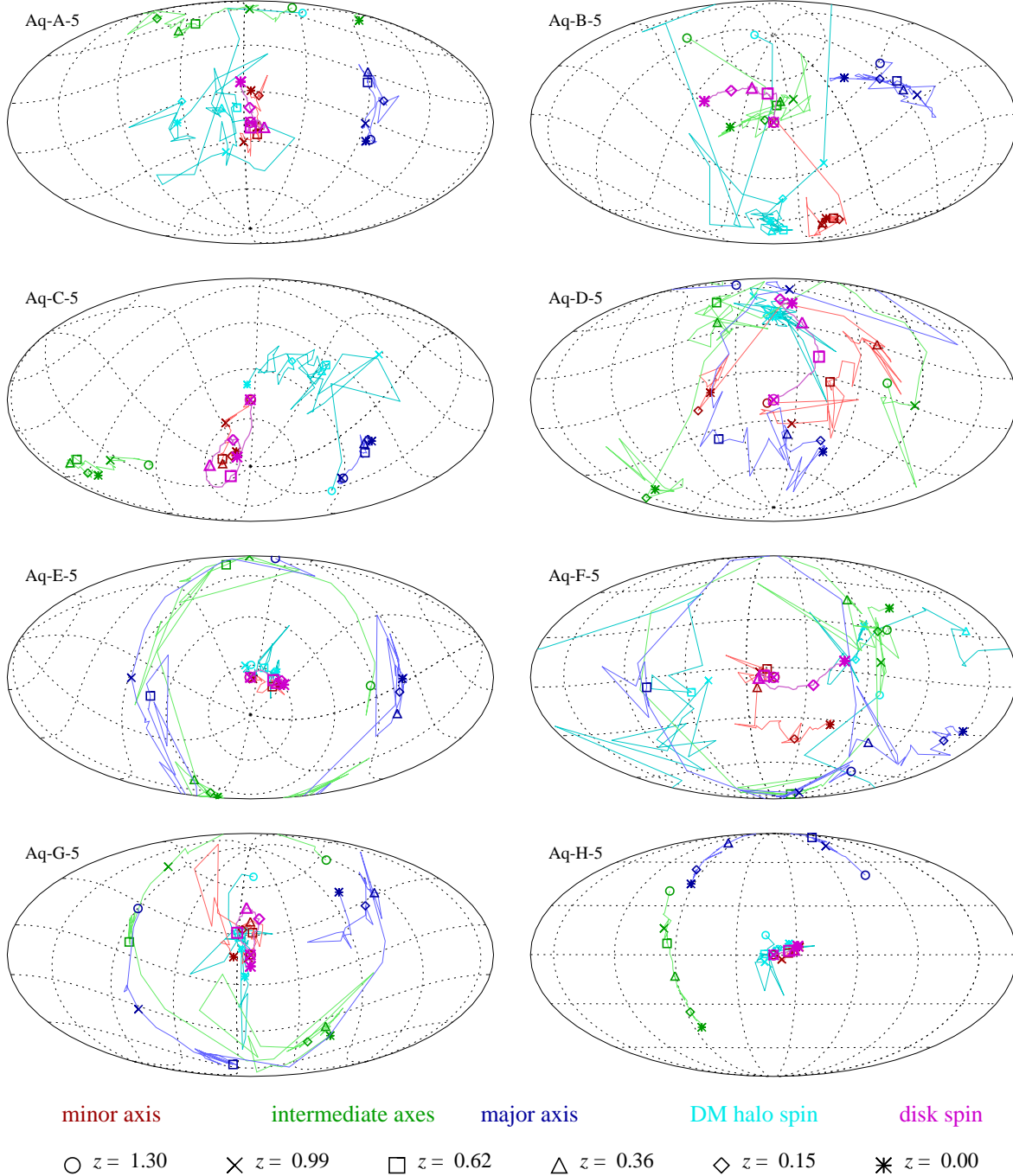


Figure 3. Orientations of the principal dark matter halo axes, the stellar disk spin vector, and the central dark matter halo angular momentum as a function of time between $z = 1.3$ and $z = 0$ in our eight Aquarius halos. In each panel, a different simulation corresponding to our default series #1 of runs is shown, as labelled. In each of the displayed runs, a pure disk is inserted at $z = 1.3$ and grown to its final mass at $z = 1.0$ keeping its shape and orientation fixed in time during the growth phase. From $z = 1.0$ to $z = 0$, the disk is evolved live. Different redshifts are singled out with symbols, as labelled. In each panel, the vector orientations are shown in a Mollweide projection of the unit sphere, with the initial orientation of the disk aligned with the centre of the map.

However, for simplicity, we have restricted ourselves to simpler models with two integrals of motion (E , L_z), implying that the radial and vertical velocity dispersions in the disk are equal.

In practice, we have used the moving-mesh code AREPO (Springel 2010) for evolving our N-body systems in time. While the hydrodynamical features of this code are not exercised in this work, its N-body solver represents an improved and more efficient real-

ization of the algorithmic methods of the GADGET code (Springel 2005), which we found convenient to make use of. In particular, the built-in parallel version of the SUBFIND algorithm (Springel et al. 2001) used to identify dark matter substructures is more efficient in AREPO than in GADGET. We run SUBFIND regularly on the fly while the N-body system is involved in order to track the masses

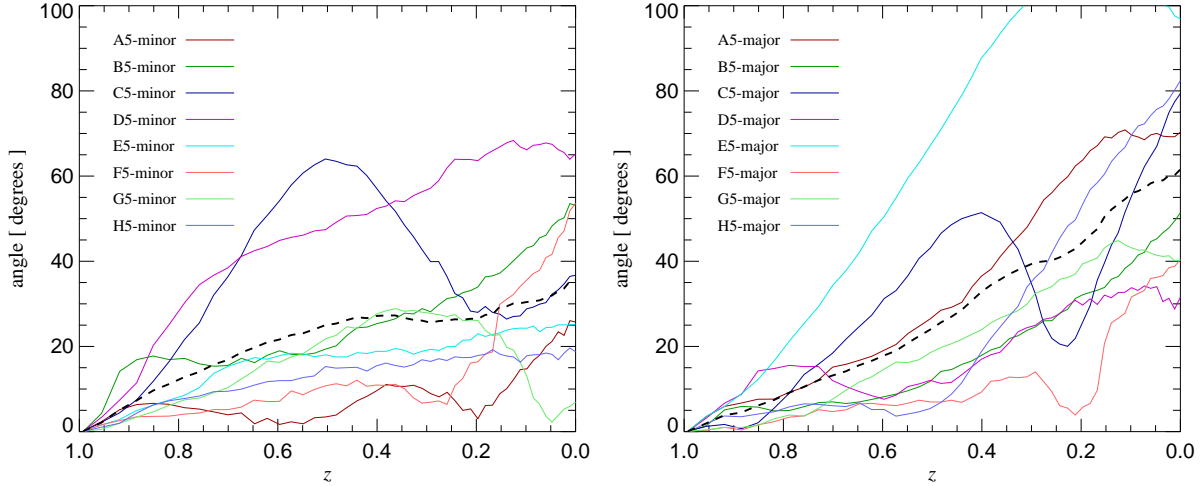


Figure 4. Angle between the current disk spin axis and the initial disk orientation when the disk goes live (at $z = 1.0$), in our default disk models of simulation series #1, as a function of time. The left panel shows our results if the disks are aligned along the minor axes of their hosting dark matter halos, the right panel is for the major axes. Most of the disk galaxies experience substantial tilting during the 7.6 Gyr of evolution from $z = 1$ to $z = 0$, independent of whether they are initially oriented along the minor or the major axis of the dark matter halo.

and positions of all halos and subhalos, as well as to measure basic dark matter halo properties such as their shape and orientations.

To facilitate the realization of a large number of disk insertion simulations, we have largely automatized the process of putting in live disks into the Aquarius halos. To this end, the cosmological simulation automatically measures the dark matter halo orientation at z_{insert} , inserts the initially rigid stellar system, and continues with the disk growth phase until z_{live} , at which point a snapshot file is written. A special version of GALIC is then started by a script that replaces the disk velocities in this snapshot file with a self-consistent stationary solution, taking the halo motion, the disk orientation, the Hubble flow at that epoch, etc., into account. Then, the AREPO simulation of the N-body system is continued from z_{live} to $z = 0$.

To determine the orientation of the dark matter halo, we calculate the principal axes of the moment-of-inertia tensor of the dark matter particles in a spherical region of size $R_{\text{vir}}/4$. By restricting ourselves to the inner region, we avoid strong influences from the less well relaxed outer parts of halos. In general, analysis of the halo shapes of CDM halos has found only mild variations of the axis ratios with radius (Allgood et al. 2006), and quite stable directions of the ellipsoidal axis (Hayashi et al. 2007). By measuring the moment-of-inertia tensor in a spherical aperture the axis ratios are biased low, but the directions of the principal axes, which is all that matters for our purposes should be unaffected and line up well with the principal axes of the halo potential. In our simulations we have aligned the spin axis of the disk either with the minor or the major axis identified in this way. The direction of the spin axis was chosen such that the angle with the dark matter angular momentum of the inner halo (again using $r < R_{200}/4$ for selecting this) was minimized. To take account of the fact that we expect the formed galaxy to be stationary in physical coordinates, we keep the gravitational softening fixed in our runs in comoving coordinates until $z = 1.5$, and fixed in physical coordinates thereafter. The same softening length is used for the stellar particles and the high-resolution dark matter particles.

The above methodology can be readily generalized to stellar

systems that include a bulge component besides a disk. To this end an additional set of particles is inserted and grown in parallel to the disk component, and GALIC then calculates initial velocities for the bulge component as well.

For test simulations, we have also implemented a “roundening” procedure for the dark matter halo. To this end, all dark matter particles contained in the friends-of-friends (FOF) group of the target halo at z_{insert} are rotated by a random angle around the halo centre, and their velocity vectors are randomized in direction in the rest frame of the halo. By construction, this procedure makes the halo spherically symmetric and smooth with isotropic distribution function while keeping the spherically averaged density profile and kinetic energy in random motions unchanged. All substructure in the FOF halo are eliminated as well. However, as a result of this procedure the halo will be slightly out of equilibrium initially. It has however enough time to relax again during the disk growth phase, so that when the disk goes live it does so in a stationary halo that is spherical apart from asymmetries induced by the disk growth itself. In a variant of this procedure, we restrict the roundening operation to just those particles bound in substructures (which amount to a few percent of the total mass of the halo). This allows the creation of dark matter host halos that retain the cosmological triaxiality but are largely pruned of dark matter substructures, at least at times close to z_{insert} . Later, new substructures will fall in due to halo growth.

3 SIMULATION SET

For definiteness and ease of comparison with DeBuhr et al. (2012), we adopt for our default disk insertion runs their choice of disk mass, $M_d = 5 \times 10^{10} M_{\odot}$, and disk scale length, $R_d = 3$ kpc. Also, we use in these default models their choices of $z_{\text{insert}} = 1.3$, $z_{\text{live}} = 1.0$, and $N_{\text{disk}} = 200,000$, combined with a canonical thickness of 0.2 times the scale length. For our adopted cosmol-

ogy¹, the growth period of the disk then lasts $T_{\text{growth}} \simeq 1$ Gyr, and the live evolution of the disk system proceeds for $T_{\text{live}} \simeq 7.6$ Gyr.

We have carried out simulations for eight different Aquarius dark matter halos, labelled A to H, following the notation of Springel et al. (2008a) and Scannapieco et al. (2009). In all of these, the pure disk models were run both with minor and major axes orientations, forming a set of 16 default models. The simulations are so-called ‘zoom-simulations’ where the mass resolution of the initial particle load has a strong spatial resolution; a high-resolution sampling of the Lagrangian region of the target halo is surrounded by shells of progressively more massive particles, so that the target halo feels the same gravitational tidal fields as if it was forming in a simulation where the whole periodic box of side-length 137 Mpc was uniformly followed at the high resolution.

In additional simulation sets, either the structural properties of the inserted galaxy models were modified, the time of the disk insertion was varied, or additional experiments like a rounding of the dark matter halo or a (partial) elimination of substructure were carried out. Most of these additional runs were only done for the minor orientation, as we generally find only small systematic differences between the minor and major orientations, with a small preference for a higher stability of the minor orientation. Finally, we have done runs at higher resolution for selected models of the A-halo, the pure disk model with the minor rotation, and also the default disk plus bulge with minor axis orientation.

Besides the default disk series, our other main series of runs consists of disk plus bulge models where the total stellar mass was kept fixed at $M_{\star} = 5 \times 10^{10} M_{\odot}$, but one third of the stellar mass was moved to a spherical stellar bulge, modelled with a Hernquist (1990) profile with scale length $a = 2$ kpc, with the rest staying in a disk with exponential surface density profile. Note that these systems still have roughly the right stellar mass expected based on abundance matching arguments for halos of this size (e.g. Guo et al. 2010; Moster et al. 2010), and the disk-to-bulge mass ratio of 2:1 is still reasonably large. In another series we have made this ratio more extreme, by exchanging the masses of disk and bulge, yielding a disk-to-bulge mass ratio of 1:2. In addition, we have considered a series of runs where only the disk mass was reduced by one third relative to our default disk model (“light disk” models) and the bulge was omitted.

Table 1 gives an overview of these different simulation sets and lists some of their most important numerical parameters. In all the runs, we have used conservative integration settings for the tree force accuracy and timestep size in order to ensure that all simulations are unaffected by orbit integration errors.

4 RESULTS FOR PURE DISK MODELS

4.1 Disk orientation and visual morphology

In Figure 1 we show projected images of the time evolution of the stellar disk material in our eight Aquarius halos, where a pure disk of mass $5 \times 10^{10} M_{\odot}$ and scale length $R_d = 3$ kpc is inserted

¹ The cosmology adopted in the Aquarius project is the same one used in the Millennium simulation (Springel et al. 2005), and is characterized by $\Omega_0 = 0.25$, $\Omega_{\Lambda} = 0.75$, $\sigma_8 = 0.9$, $n_s = 1.0$, and a Hubble constant of $H_0 = 73 \text{ km s}^{-1} \text{ Mpc}^{-1}$, consistent with the WMAP-1 and WMAP-5 cosmological constraints. The small offset of the cosmological parameters with the most recent determinations by Planck does not matter for the purposes of this study.

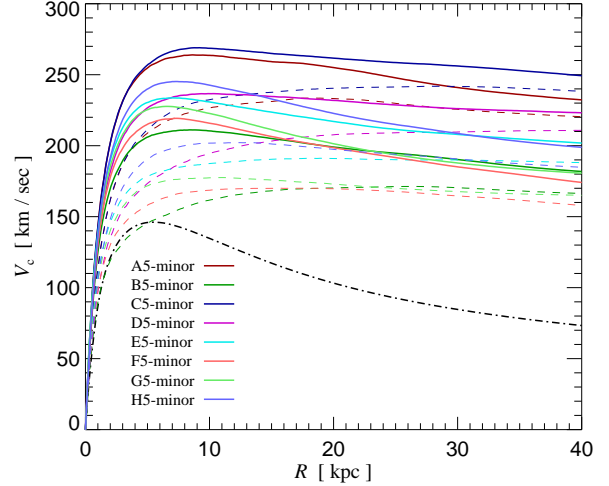


Figure 5. Rotation curves of our default disk models (series #1) at redshift $z = 1$, when the disk goes live. The rotation curve velocity is here defined based on the enclosed mass at a given radius. Note that the disk is kept the same in all these eight simulations, hence its contribution to the rotation curve (dot-dashed line) is always the same. The dashed lines show the contributions of the different dark matter halos, while the solid curves give the total rotation curves of the eight systems, with different colours as specified in the legend.

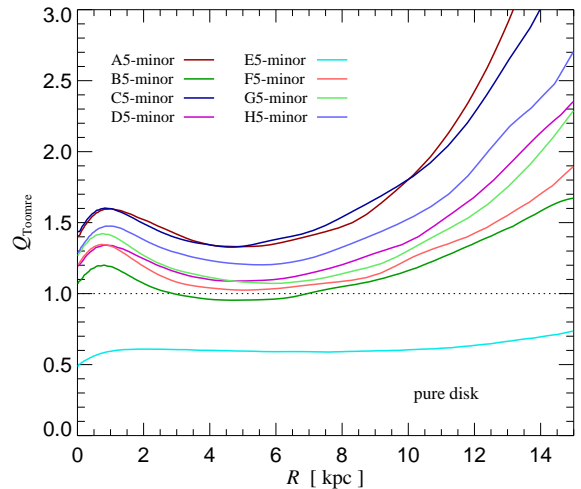


Figure 6. Radial run of Toomre’s Q-parameter (Toomre 1964) for axisymmetric stability for our disk simulations of series #1, at $z_{\text{live}} = 1$. Model B5 is expected to be marginally unstable against axisymmetric instabilities, whereas E5 should be strongly unstable. Evidence for this is in fact seen in Figure 1, where E5 shows residual axisymmetric ring-like features in its disk at $z = 0.85$ that are not present in this form in the other runs.

along the minor axis of the halos. In each individual panel of the figure, the disk stars have been turned to a face-on orientation, taking the spin angular momentum of the stars in the central region of the disk (within 5 kpc) to define the disk normal. All the models almost immediately form very strong bars, consistent with the findings of DeBuhr et al. (2012) for halos A–D. This bar instability can be understood as an early response of the disk to the asymmetry of the dark matter distribution (Romano-Díaz et al. 2008).

When viewed in an edge-orientation, as shown in Figure 2, a planar disk-like distribution of the majority of stars is maintained in all the cases, but the presence of the strong bars is clearly revealed by pronounced X-shaped features in the centre of the galaxies. It is also evident that the disks are thickened to different degrees. Halo E sports a particularly thick disk at the end, and some systems, notably halos B and F, show substantial bending in the periphery of the disks. Nevertheless, the amount of stellar material significantly outside the disk plane seems to be rather limited, somewhat different from the findings of DeBuhr et al. (2012) for halos A-D.

The equivalent simulations for inserting the disks along the major orientation of the halos (series #2) yield qualitatively very similar results, and we therefore refrain from showing the corresponding images. Figure 3 gives instead an overview of the time evolution of the orientation of the halos' minor, major and intermediate axes, as defined based on the moment of inertia tensor of the central dark matter distribution in a spherical aperture of size $R_{200}/4$. We also include in the plots the evolving orientation of the disk spin axis as a function of time (based on the minor orientation runs of series #1), as well as the dark matter spin direction of the central region of the halo. The individual panels are Mollweide projections of the corresponding direction angles, one for each Aquarius halo. The origin of the projection has been shifted such that the initial position of the disk orientation lies at the center of the corresponding Mollweide map.

Interestingly, in several of the systems, the dark matter halo spin is quite well aligned with the minor axis. This is in particular the case for systems A, E, G, and H, and to a lesser degree in B. In halos C and D, the dark matter spin is reasonably stable in orientation but offset from the minor axis, while in F it wanders all over the place. Studies of cosmological halos have long found a preference of the dark matter halo spin to line up with the minor axis (e.g. Hayashi et al. 2007), a trend also seen here. Interestingly, there is growing observational evidence from alignment studies of SDSS galaxies (Zhang et al. 2015) that favor a picture where disk spins line up with the dark matter halo angular momentum of the inner regions of halos, suggesting that the minor orientation arises naturally and is actually preferred. Moreover, Aumer & White (2013) found in their idealized baryonic simulations of disk formation that disks indeed are most stable if the spin of the disk is aligned with the minor axis of the halo.

What is also evident from Figure 3 is that the disk spins of several of the models wander away significantly from their original orientation, especially in those cases where the minor axis shows a change of orientation as well. Of course, the change of spin orientation arises from gravitational torques, similar to how a spinning top precesses in an external field (Landau & Lifshitz 1969), but the detailed evolution of the live stellar disks is more complicated to understand due to the large-scale gravitational torques acting on the galaxy, as well as due to the coupling of the disk and the triaxial halo. In cases where the minor axis moves little, such as E and H, the disk spin exhibits a fairly stable orientation (see also Debattista et al. 2013). A clearer view of the size of the changes in orientation is given in Figure 4, where the angle between the current disk orientation and its initial orientation is shown as a function of time, from redshift $z = 1$ to $z = 0$. The left panel shows our results when the disk is initially aligned with the minor orientation, the right panel is for the major orientation. Some of the models show rather substantial reorientations of the disks reaching up to 65 degrees in the minor cases, and even larger angles beyond 110 degrees for the major orientation. The average tumbling angle (shown as a dashed line) for the eight systems is 35 degrees for the minor

orientation, and 60 degrees for the major orientation. The substantially smaller average tilt angle for the minor orientation suggests that this orientation typically offers better long-term directional stability than the major orientation, as expected. We note that our results for A-D show a large resemblance to those of DeBuhr et al. (2012), for example, we find the same characteristic evolution pattern for halos A and C. This is reassuring, given the independent and at a technical level quite different methodology to introduce and simulate the live disks. However, there are also some quantitative differences, and for a subset of the systems we tend to find somewhat smaller angles than DeBuhr et al. (2012).

4.2 Radial and vertical structure, and its evolution

As pointed out by DeBuhr et al. (2012), it is perhaps not too surprising that these systems show such strong tendencies to form bars. Whereas their rotation curve structure, shown in Figure 5, in principle suggests that the disks are not exceeding the rotation curve contribution of the dark matter anywhere (apart from halo G for a small region) and are thus far away from being maximal disks, the simple criterion of Efstathiou et al. (1982) for stability against bar formation,

$$Q_{\text{bar}} \equiv \frac{v_{\text{max}}}{(GM_d/R_d)^{1/2}} > 1.1 \quad (1)$$

is violated for all the models. Here v_{max} is the maximum rotation curve velocity, and M_d and R_d refer to mass and scale-length of the exponential stellar disk. In fact, the values for Q_{bar} after the disks have been inserted are 0.99, 0.79, 1.0, 0.88, 0.87, 0.82, 0.85, and 0.92, for A to H, respectively.

It should be noted however that the simple criterion of Equation (1) is not particularly reliable in general disk systems. In fact, Athanassoula (2008) has given a number of counter-examples that violate this criterion for bar instability. For example, if a disk is supported by a high radial velocity dispersion it can evade forming a bar even if the criterion by Efstathiou et al. (1982) is violated. Similarly, Athanassoula & Misiriotis (2002) have shown examples for bar growth in massive, quite concentrated halos where this would have been unexpected according to the criterion. However, our disk systems were all initialized as isotropic rotators, and hence form a more restricted class of models for which Equation (1) can still be useful to assess the relative susceptibility to bar formation.

In this context it is also interesting to look at Toomre's stability parameter for axisymmetric stability of stellar disks (Toomre 1964),

$$Q_{\text{Toomre}} \equiv \frac{\sigma_R \kappa}{3.36 G \Sigma} > 1, \quad (2)$$

where σ_R is the radial velocity dispersion, Σ the surface density, and

$$\kappa^2 = \frac{3}{R} \frac{\partial \Phi}{\partial R} + \frac{\partial^2 \Phi}{\partial R^2} \quad (3)$$

is the epicycle frequency. The value of Q_{Toomre} is shown as a function of radius in Figure 6. Interestingly, most of the models are Toomre stable, with B and F being marginal cases, but the light halo E is clearly predicted to be unstable against axisymmetric instabilities. And indeed, inspecting the stellar images at $z = 0.85$ in Fig. 1 one can clearly see ring-like spherical features that are absent in this form in the other models, providing evidence that such instabilities have occurred in the early evolution of the system.

We find further signs for this special evolution of halo E in the evolution of the structural properties of the systems, which we

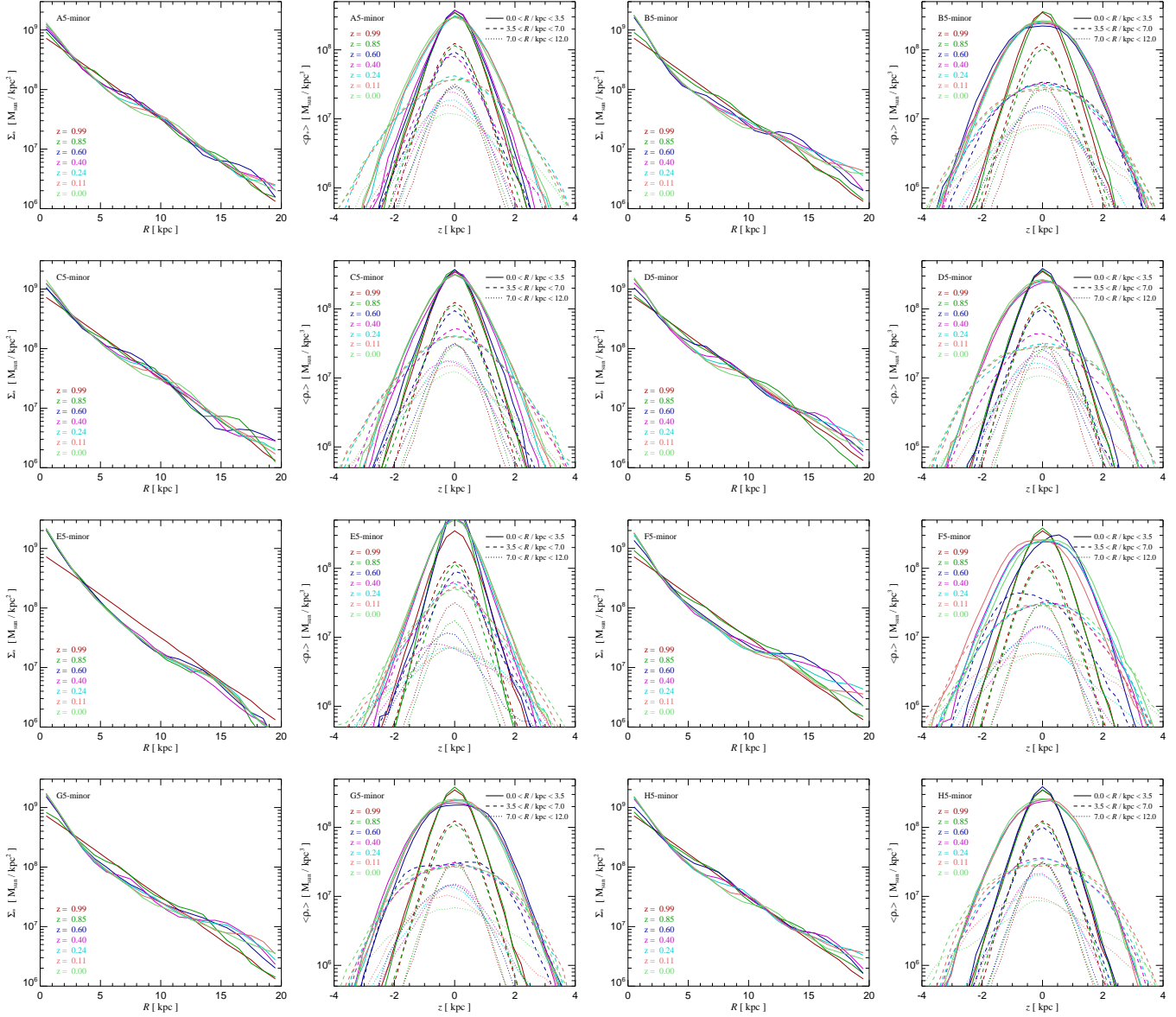


Figure 7. Radial and vertical disk density profiles for our default disk simulations (series #1) as a function of time. We show results for all of our eight Aquarius halos, in each case with a pair of panels where the surface density profile is shown on the left, and the vertical density profiles on the right. For the latter, three families of curves are shown, corresponding to averages over different radial ranges ($R < 3.5$ kpc, 3.5 kpc $< R < 7.0$ kpc, and 7.0 kpc $< R < 12.0$ kpc, as labelled). In all panels, the initial density distribution when the disk goes live is shown together with 6 subsequent times down to $z = 0$, and at each time, the disk plane has been defined based on the angular momentum of the stars in the inner 5 kpc.

examine next. In Figure 7 we show the radial and vertical density profiles, at a set of different times. The exponential surface density profile measured for the face-on orientation of the disks is quite robust and more or less retains its initial shape, despite the rather dramatic bar formation events occurring in these simulations. In contrast, the vertical density profiles (three families of curves are shown, corresponding to different radial ranges, as labelled) show the damaging impact of the forming bars more clearly. In particular, a relatively sudden transition to a new vertical equilibrium with a thicker profile is apparent in most of the models. One interesting difference with DeBuhr et al. (2012) is that our models A–D show substantially less broadening in the outer parts of the disks. This is

presumably a reflection of our more accurate approach to initialize the velocities of the initial disk models.

Further support for this is provided by the evolution of kinematic quantities, for example those shown in Figure 8. The eight panels on top in the figure give the evolution of the profiles of the vertical velocity dispersion σ_z^2 , while the bottom eight measure the disk height in terms of the median $z_{1/2}$ of the absolute value of the vertical z -coordinates of the star particles relative to the disk plane. Or in other words, half of the stellar mass has a height above the central disk plane less than $z_{1/2}$. Comparing again to DeBuhr et al. (2012), we see that our $\sigma_z(r)$ profile at $z = 0.85$ is much closer to the initial profile than in their case, suggesting that our disk models are in better dynamical equilibrium initially. This equilibrium

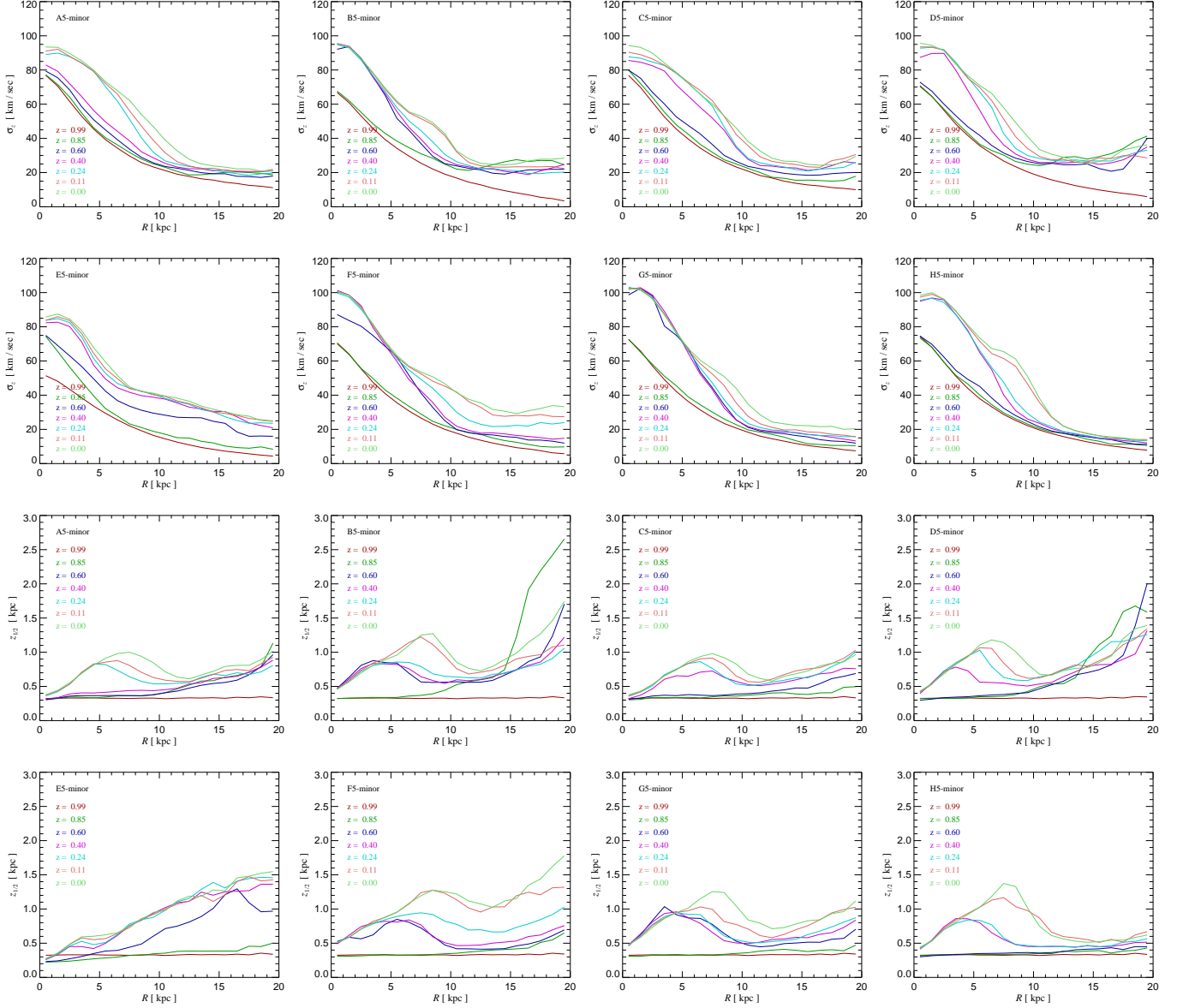


Figure 8. Evolution of the vertical velocity dispersion profile and of the half-mass height profile of the disk particles in our default disk insertion simulations (series #1). The top panels give the expectation value of the vertical stellar velocity $\sigma_z = \langle v_z^2 \rangle^{1/2}$ measured in different cylindrical shells aligned with the stellar spin axis of the stars at the corresponding times. The height profiles give the median of $|z|$ relative to the disk plane, i.e. half the stars have distances below/above $z_{1/2}$ from the disk plane.

is however anyway destroyed relatively quickly by the onset of bar formation. Another notable difference are the much smaller values for $z_{1/2}$ we find in the outer parts of the disks, corroborating the observation that our disk models appear to be in better equilibrium.

4.3 Bar strength and vertical heating

The formation of the bar can also be studied more quantitatively, for example through measuring a bar strength indicator, or by looking at the vertical heating of the stellar disk. As a simple global measure of the total amount of vertical heating we can use the quantity

$$\zeta = \frac{\langle v_z^2 \rangle}{\langle v_z^2 \rangle_0}, \quad (4)$$

which simply is equal to the total kinetic energy in vertical motion relative to the initial value of this quantity at the time the disk starts to evolve live.

As a characterization of the bar strength, we adopt a simple measure for the $m = 2$ Fourier mode of the disk, as is often done to quantify bars. For definiteness and ease of comparison, we measure the bar strength similarly as DeBuhr et al. (2012), by first determining the quantities

$$a_2^{(b)} = \sum_{i \in b} m_i \cos(2\phi_i) \quad (5)$$

$$b_2^{(b)} = \sum_{i \in b} m_i \sin(2\phi_i) \quad (6)$$

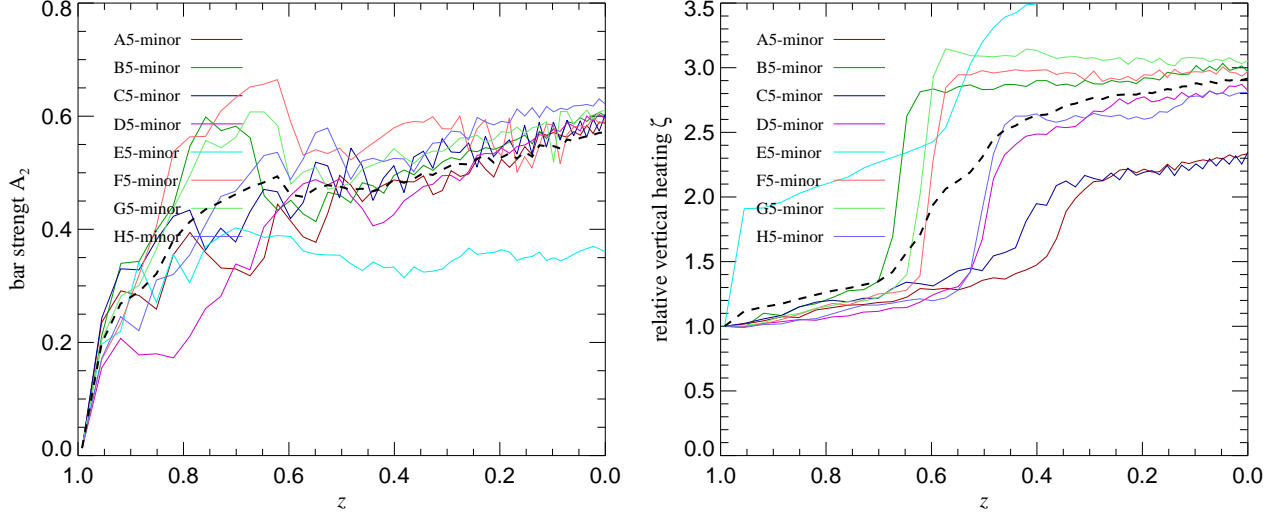


Figure 9. Bar strength parameter A_2 (left panel) and relative vertical heating (right panel) in the simulations of our default pure disk insertion simulations (series #1), as a function of time. It is clearly seen that all the models develop a strong bar characterized by $A_2 \simeq 0.6$, except for model E, which yields $A_2 \sim 0.3$ at the end. The latter model is special as it shows substantial vertical heating right after the disk becomes live. This is because this system is unstable against axisymmetric instabilities (see Fig. 6). The dashed lines in the two panels illustrate the average simulation behaviour.

for a set of 30 radial bins between $R = 0$ and $R = 2 R_d = 6$ kpc. Here ϕ_i refers to the azimuthal angle of each disk star, and the sums extend only over the particles in a radial bin b . Defining $c_2 = \sqrt{a_2^2 + b_2^2}$, we then calculate a bar strength parameter as

$$A_2 = \frac{\sum_b R_b c_2^{(b)}}{\sum_b R'_b M'_b} \quad (7)$$

where M_b is the mass falling into bin b , and R_b is the bin radius.

In Figure 9, we show our results for the time evolution of the A_2 parameter in the left panel, and in the right panel we give the time evolution of the vertical heating parameter ζ . Consistent with the evolution of the visual morphology, all the systems show a rapidly growing bar signal in their early evolution, with all the models except E converging to a similarly high bar strength of $A_2 \simeq 0.6$ at the end.

Interestingly, the relative vertical heating parameter shows only a small and slow growth in the beginning, but then jumps up rapidly by a large factor, followed by a stabilization at a new high level. In contrast, the bar strength indicator becomes high already significantly earlier. Presumably this is a combination of two different effects. One is that some disk asymmetries quickly develop in the early disk evolution simply because of the non-sphericity of the halo potential, which for example manifests itself in pronounced spiral patterns in the disks. The other is that during the initial phase of bar formation the density contrast of the bar grows without yet leading to a notable change in the vertical structure. Only later, once the bar ‘‘collapses’’ or buckles, a sudden transition to a new equilibrium occurs, and this is associated with some degree of violent relaxation and significant vertical heating (e.g. Martinez-Valpuesta et al. 2006; Berentzen et al. 2006).

5 MODELS WITH BULGES AND LIGHTER DISKS

The strong bars formed in the models considered in the previous section raise the question under which conditions disk galaxies

could survive in the Aquarius halos and maintain a nice, disk morphology all the way to $z = 0$. It appears clear from the preceding results that the bar criterion of Efstathiou et al. (1982) should be taken as an important first guide. Increasing the value of Q_{bar} in a given dark matter halo can be achieved first of all by making the disk lighter, and/or by making it larger. However, we note that there is only limited room for such changes if one wants to keep the disk parameters close to observational inferences, such as the stellar mass–halo mass relationship derived from abundance matching (Guo et al. 2010; Moster et al. 2010), or direct constraints on the size–stellar mass relationship (Shen et al. 2003). Another problematic aspect of simply adopting a very light disk is that this will greatly reduce the rounding effects of the dark matter halo due to the growth of a baryonic mass distribution in the centre. Such a rounding is however essential to keep the destructive effects of a highly triaxial dark matter potential on disk stability and morphology at bay.

Another approach to improve the stability of the disk against bar formation is to add a central stellar bulge in addition to the disk. Such a bulge increases the circular velocity of the spheroidal component of the system, i.e. it contributes to the numerator of the bar stability criterion. At the same time, growing a central spherical bulge in a dark matter halo is an effective way to rounden the dark matter potential. Of course, on the other hand, adding a central bulge is limited by the observed bulge-to-disk ratios, and is not a promising option for explaining pure disk galaxies.

To test these options, we have considered a few additional sets of runs. Our default standard bulge models (series #3) have the same stellar mass as our default disk models, but one third of the stellar mass is put into a bulge, with two thirds remaining in the disk. Such bulge-to-disk ratios are about the smallest ones that the present generation of hydrodynamical simulations of disk formation can achieve (e.g. Marinacci et al. 2014a).

In addition, we have also run models where we omitted this bulge, which is exploring the lighter disk option at some level. Here the disk mass was reduced to 2/3 of the value in our default models

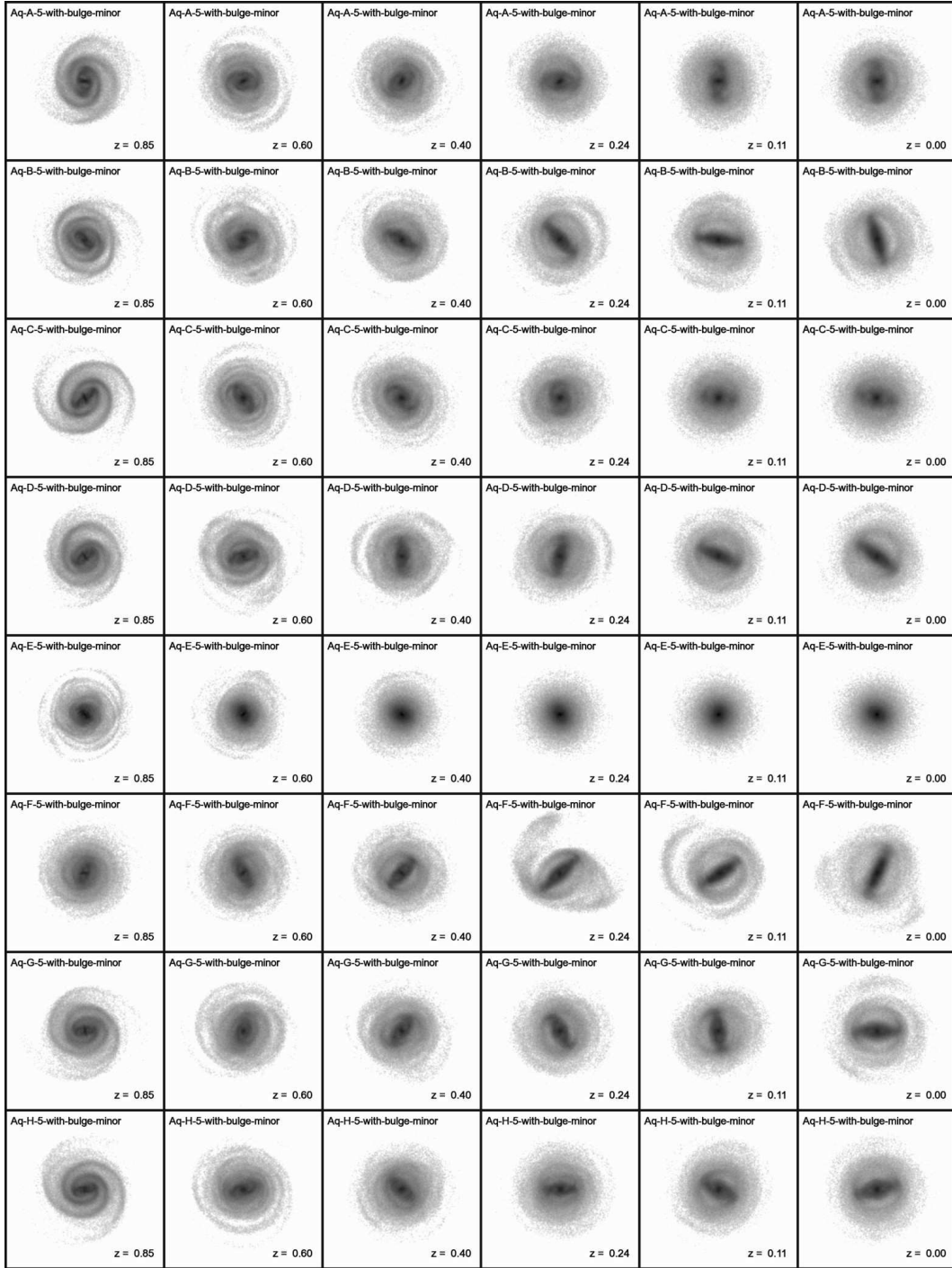


Figure 10. Face-on projections of the stellar mass of the disks in our runs with bulges (series #3), where one third of the stellar mass is moved to a central spheroidal bulge and two thirds are kept in the disk. Otherwise, the outline of the figures and the image generation method corresponds exactly to that of Fig. 1.

(series #4). This is complemented by a further set of runs in which we swapped the masses of disk and bulge of our standard bulge models, ending up with 1/3 in the disk and 2/3 in the bulge (series #5). We would expect these models to be extraordinarily stable against bar formation.

Finally, to test the influence of the residual triaxiality of the dark matter halos on the disk stability, we have also run two sets of simulations where we artificially sphericalized the dark matter

halos at the instant of disk insertion, i.e. at $z = 1.3$ (series #6 and #7). To this end, we simply took all dark matter particles in the FOF halo at that time and rotated them randomly around the halo center. Also, their velocities were isotropized by turning them randomly in the rest frame of the halo. In this way, the density structure and potential energy of the halo was approximately maintained, with any deviation from non-equilibrium decaying away during the disk growth phase. When the disk goes live at $z = 1.0$ it then does so

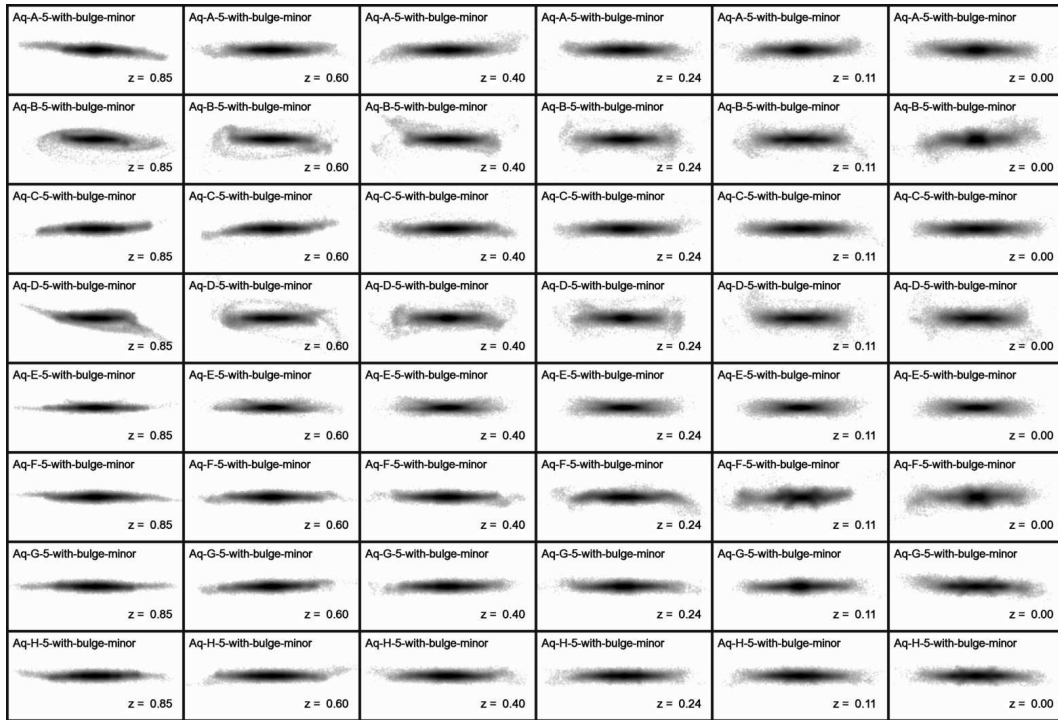


Figure 11. Edge-on projections of the stellar disks in our runs with bulges, giving the side-views of the corresponding images shown in Figure 10. As in the corresponding images of Fig. 2, each panel has an unchanged physical size in the horizontal direction (54 kpc) and uses an identical colour-scale as in the face-on images.

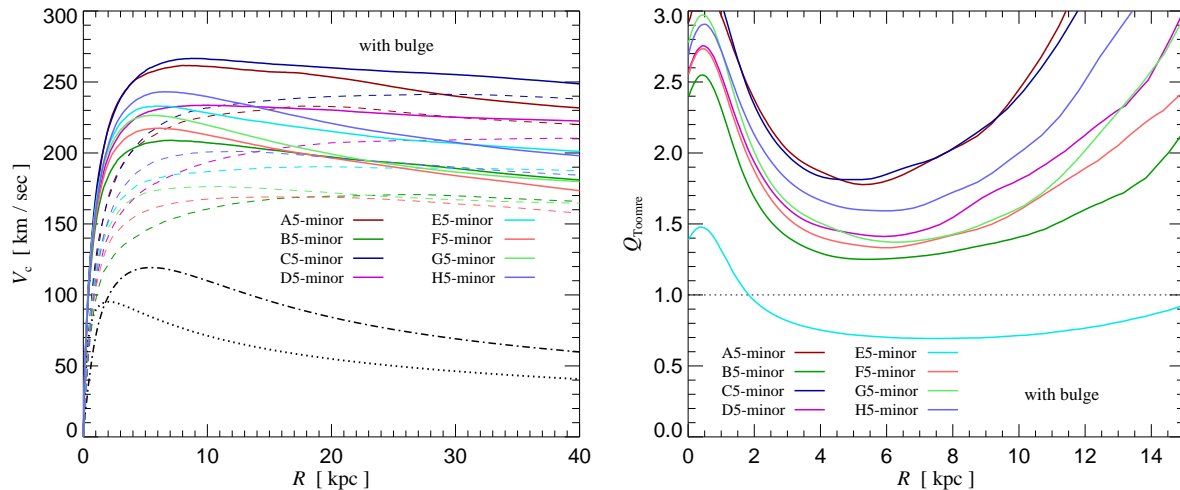


Figure 12. Rotation curves and Toomre- Q stability parameter of our default simulations with bulges (series #3), as a function of radius. The left panel shows the rotation curves, where the disk (dot-dashed) and bulge (dotted) always make the same contributions due to their constant parameters. The different dark matter halo contributions are shown by dashed lines, and the total rotation curves by solid lines. The panel on the right illustrates the expected stability against axisymmetric instabilities. While the bulge has a substantial stabilizing influence (compare to Fig. 6), model E5 is still found to be unstable for the adopted stellar parameters of disk and bulge.

in an essentially spherical halo, but the mass growth of the halo, including the accretion of newly infalling substructures on to the halo, stays unaffected.

We begin our review of the results of these runs with images of the disks in the runs with the small bulges. These are shown in face-on and edge-on orientations in Figures 10 and 11, respectively. Note that the bulge stars are not included in these images.

Compared to the corresponding images for the simulations with pure disk, the disks are clearly much less effected by bulge formation, although most systems still do form bars, albeit of weaker strength and at later times. The edge-on projects of the disk stars correspondingly show much less evidence for central bars.

The rotation curves of the models with bulges, as well as the corresponding profiles of the Toomre stability parameter are shown

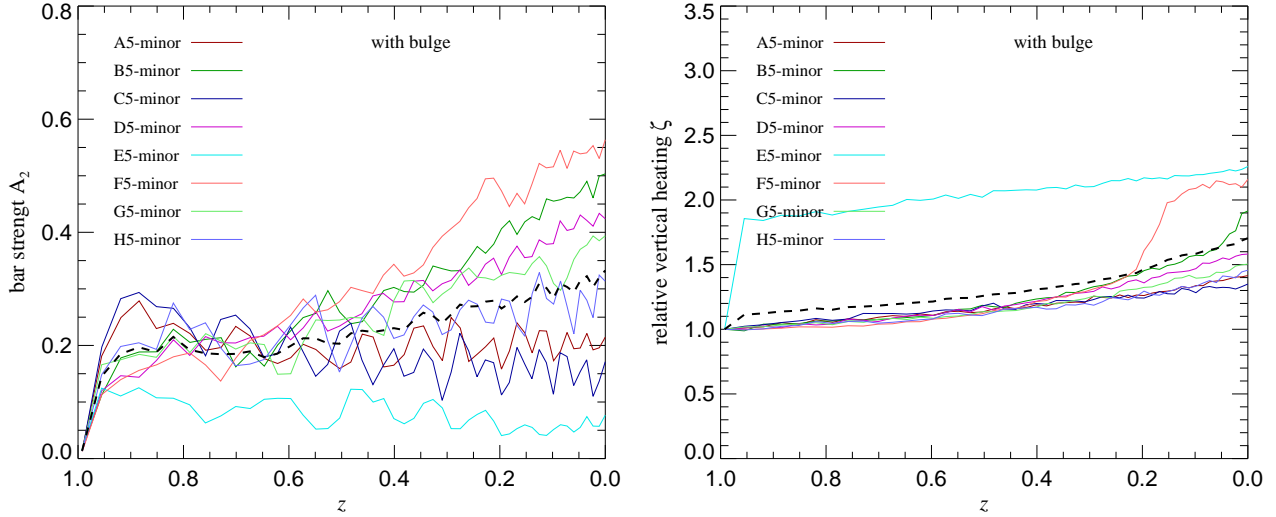


Figure 13. Bar strength parameter A_2 (left panel) and relative vertical heating (right panel) in our default disk+bulge simulations (series #3), as a function of time. These evolutions can be directly compared to the corresponding results for the pure disk case shown in Fig. 9. Now only a subset of the systems develops bars, and even if this happens, the bars are weaker and form later. Model E still appears as an outlier, caused by its instability against axisymmetric perturbations. We note that the early growth of the A_2 indicator to values of around ~ 0.2 does not really measure a bar; it is presumably caused by a quick distortion of the spherical disk into an ellipsoidal disk due to the residual asymmetry of the dark matter halo potential.

in Figure 12. None of the models is any more dominated by baryons at any radius, and as expected, the resistance against axisymmetric instabilities is increased substantially. Note however that halo E is still predicted to be Toomre unstable. This is confirmed by visual inspection of simulation E at $z = 0.85$ in Fig. 10, which reveals conspicuous axisymmetric rings of stars.

The weaker bar strengths in the bulge-runs also become evident in Figure 13, which shows the time evolution of the bar strength parameter A_2 and the vertical heating parameter ξ of the disks of our eight standard bulge models. Comparing to the corresponding results for the pure disk models (Fig. 9) clearly shows a much weaker trend towards making strong bars. Most notably the early evolution is very different, where all the models show a small value of A_2 as a result of deviations from axisymmetry due to the aspherical dark halo potential, but no strong bulge signal is present yet. Only after a few Gyr, a subset of the models starts to grow a significant bar.

It is also interesting to examine differences in the evolution of the structural properties of the models with bulges. This is shown in Figure 14 in terms of the radial and vertical density profiles, and in Figure 15 in terms of the vertical velocity dispersion and half mass height as a function of radius. We see a very substantial improvement in the structural stability of the models with respect to the runs with pure disks. This is reflecting both, the stronger stability against bar formation, and the slightly rounder dark matter halo potential due to the more concentrated distribution of the baryons.

Getting almost completely rid of the bars is achieved in our models that adopt a massive bulge and a light disk (series #5). Here the disk images show a remarkable degree of stability. For conciseness, we refrain from showing their uneventful time evolution. Instead, we collect all our simulations in a single plot of the bar strength versus the initial Q_{bar} -parameter of Efstathiou et al. (1982), allowing us to assess how well this venerable criterion works in the context of full cosmological CDM models. Figure 16 compiles our different runs, with the bar strength A_2 measured at

$z = 0$, and the Q_{bar} -parameter evaluated at $z = 1.0$ when the disk goes live. Remarkably, the threshold value 1.1 originally introduced by Efstathiou et al. (1982) for the dividing line between bar-unstable and stable models still serves as a surprisingly robust indicator, even in the light of all sorts of other complicating factors. In particular, we note that the different symbols in the figure show a broad range of simulation models, including runs with and without bulge, with minor or major axis orientation, with ordinary or artificially rounded dark matter halos, etc. Irrespective of these factors, it appears that the strength of the disk self-gravity relative to the supporting spheroidal potential is by far the most decisive parameter for governing stability against the formation of strong bars. We note that this therefore cannot be ignored in the interpretation of mass models derived for the Milky Way. For example, the rotation curve decomposition derived by Bovy & Rix (2013) suggests that the corresponding live galaxy model should be violently bar unstable according to our results.

In light of these differences, it is now interesting to consider the stability of these models with respect to the spatial orientation of the disks. In Figure 17 we show results for several of our modified runs, including the ones with lighter disks, the ones with a bulge, the ones with a very massive bulge, and the ones for a rounded dark matter halo. The latter are for the pure disk case (series #6), but the results for the bulge case (series #7) look essentially identical.

Comparing with the corresponding results in Fig. 4 for the pure disk case, it is evident that the amount of disk tumbling is fairly independent of the structural properties of the galaxies. In particular, it does not matter much whether a bar is present or not. Apparently, the reorientation of the disk is primarily controlled by the tumbling of the dark matter halo and the torques it exerts on the disk, and this is only marginally affected by the growth of the baryonic disk/bulge system. Only when the halos are artificially rounded and any figure rotation of the inner dark matter halo is stopped by construction, the disk orientation remains stationary.

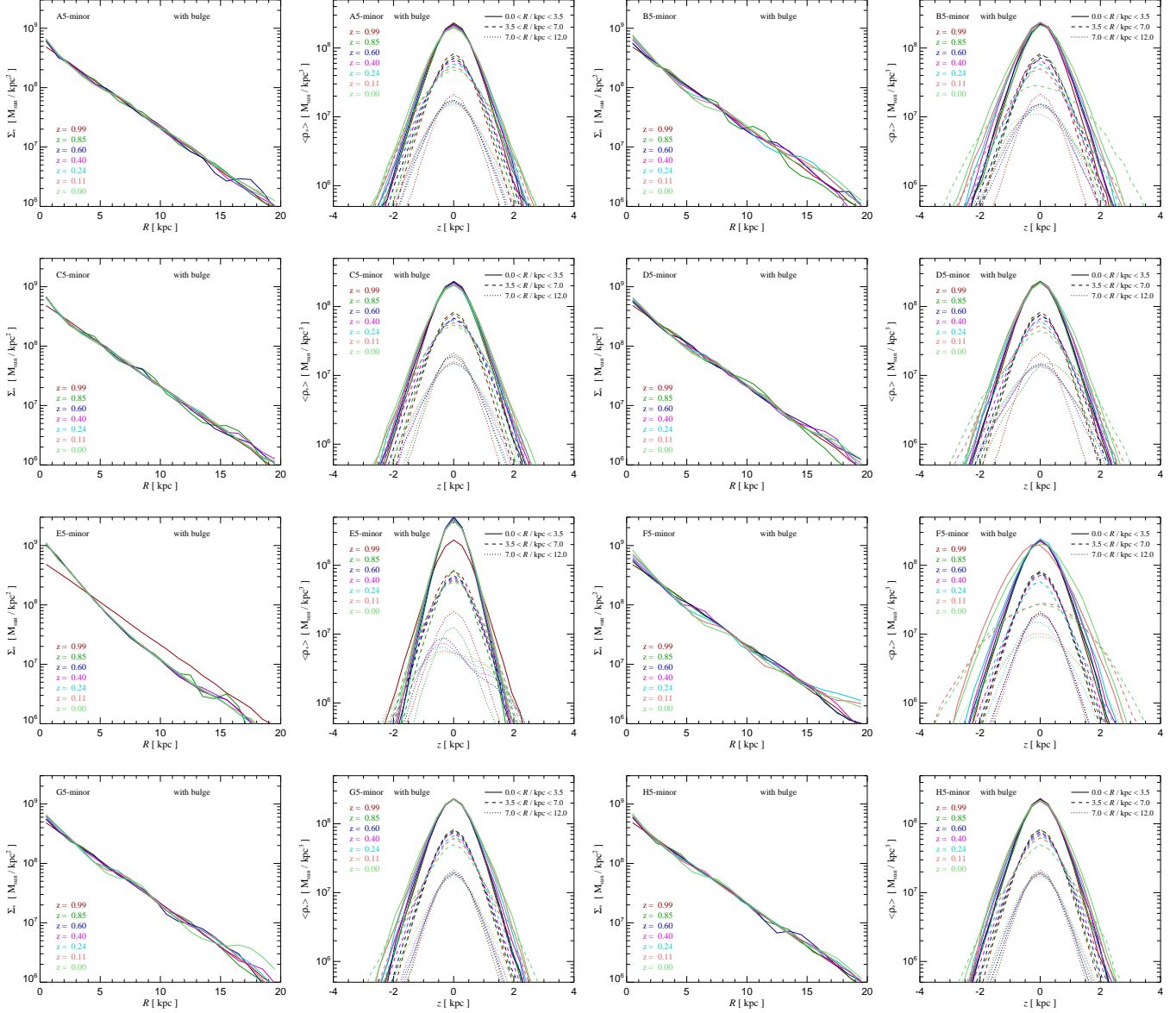


Figure 14. Radial and vertical disk density profiles for our default disk+bulge simulations (series #3) as a function of time. As in the corresponding Fig. 7 for the pure disk runs, we show results for all of our eight Aquarius halos, in each case with a pair of panels where the surface density profile is shown on the left, and the vertical density profiles on the right. Especially in the much more modest evolution of the vertical structure it is evident that these disks evolve comparatively little; i.e. the bulge has largely stabilized the disks against strong bar formation.

Except for halo F – its disk turns even in this case by a substantial angle, starting at $z \simeq 0.35$. The same characteristic turning motion of F-disks is also seen in the standard runs at this time, indicating that this is caused by the fly-by of a massive substructure that interacts with the disk at this time and torques it substantially.

The results above suggest that disk tumbling of significant size is virtually inevitable in CDM halos. We expect typical tumbling rates of about 40 degrees from $z = 1$ to $z = 0$, or about $\sim 6 - 7$ degrees per Gigayear on average. Some systems may have up to 2-3 times that, while others stay below it by a similar factor. Occasionally, disks may also be brought into a turning motion by a close encounters with a substructure. Importantly, our results show that disks can survive such reorientations largely unaffected, i.e. they

are not in apparent conflict with the observed abundance of thin stellar disks.

6 IMPACT OF SUBSTRUCTURES

Cold dark matter subhalos contain a large amount of substructures, raising the question whether they may interfere with the stability of cold stellar disks and induce substantial heating. We note however that it is well established that substructures populate primarily the outer parts of dark matter halos (e.g. Ghigna et al. 1998; Diemand et al. 2004; Springel et al. 2008a), leaving the inner halo relatively smooth. Also, the subhalo mass function is skewed very slightly to being dominated by the most massive subhalo systems.

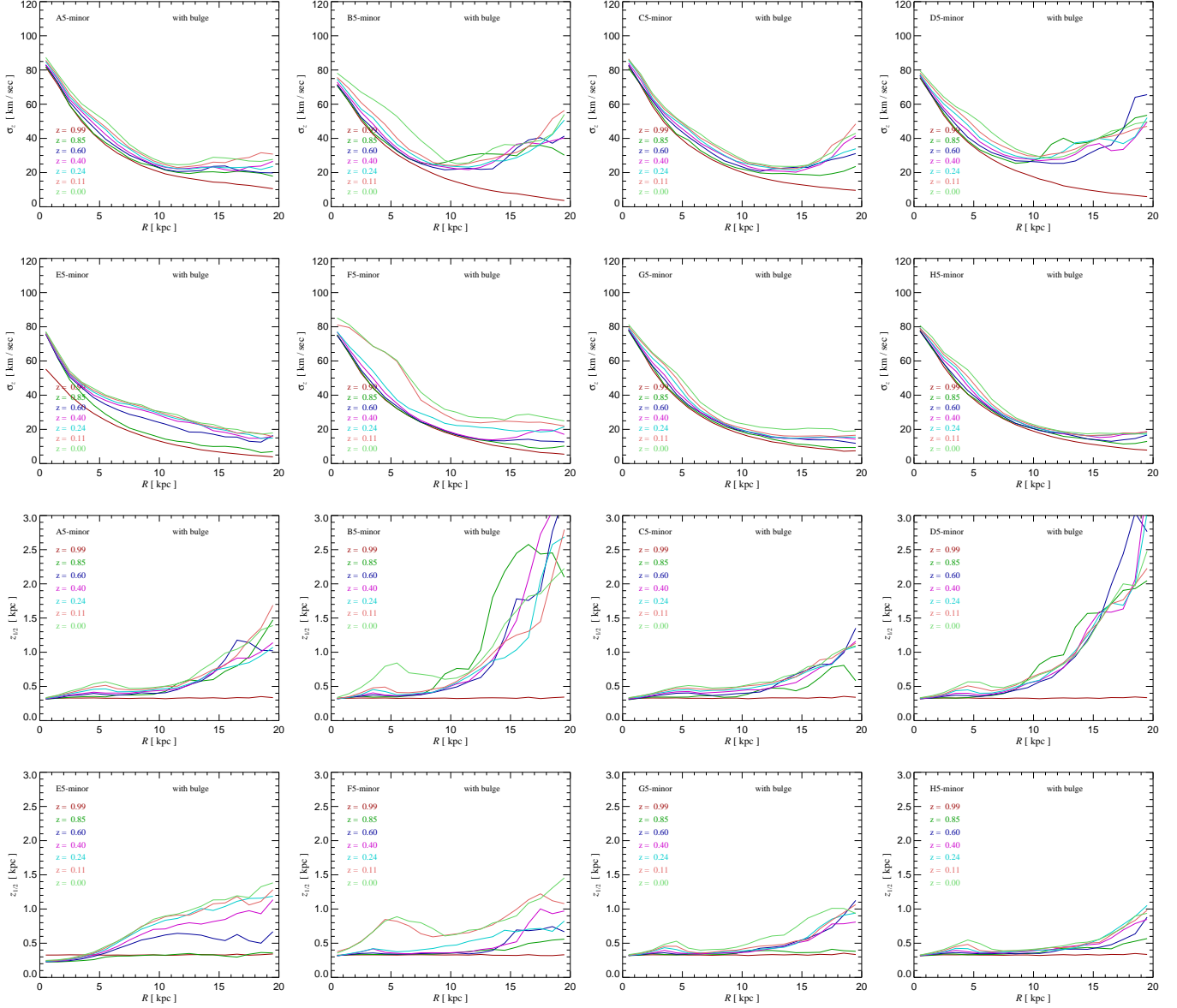


Figure 15. Time evolution of the vertical velocity dispersion profile and of the half-mass height profile of the disk particles in our default disk+bulge simulations (series #3). These results correspond directly to the simulations for our pure disk simulations shown in Fig. 8. Note that only disk star particles are included in the measurements.

Those are expected to dominate the heating (Springel et al. 2008a), but their number is small.

We here use our models to check whether subhalos contribute significantly to the disk heating, and whether the disk in turn plays a significant role in reducing substructure abundance when they pass through pericenter and experience gravitational tidal shocks from the disk or the enhanced central cusp. There is a body of previous work on this subject (e.g. Kazantzidis et al. 2008, 2009; Purcell et al. 2009; D’Onghia et al. 2010), largely based on much simpler toy simulations than studied here. Our analysis is so far the most elaborate attempt to study this in the correct cosmological setting, and in particular takes the expected system-to-system variation into account.

We consider first the subhalo abundance in runs without any disk (i.e. these are *dark-matter only* runs of A to H at $z = 0$), and

compare it to the one found at $z = 0$ in our default runs with disk. In Figure 18, we show the cumulative abundance of substructures as a function of mass in both types of simulations. To emphasize the mean difference in a clear way we show the averaged abundance over all eight systems we simulated; we note that orienting the disk along minor or major axis makes no difference here. There is a $\sim 30\%$ reduction of substructure abundance across all mass scales in the runs with the disk. This can be understood as an effect of accelerated substructure depletion due to the gravitational shocks the substructures experience as they pass through the disk. This enhanced destruction rate shows up particularly strongly in the halo center, as evidenced by Figure 19, which gives the cumulative average abundance of substructures with mass larger than $6 \times 10^7 M_\odot$ as a function of radius. In the inner parts of the halo, there is about a factor of two reduction of the subhalo abundance. These results

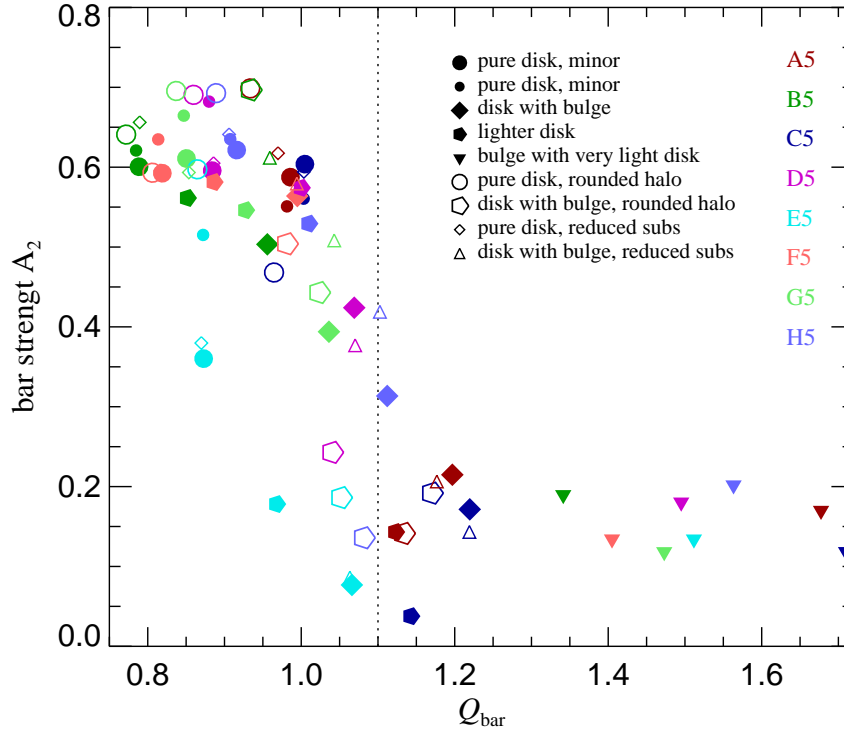


Figure 16. Compilation of the measured bar strength parameter A_2 at $z = 0$ in our simulation set versus the Q_{bar} parameter of Efstathiou et al. (1982). We here collect results for all of our runs (except for the late insertion and reorientation ones). Different colours are used for the different Aquarius halos, and different symbols for the different simulation series, as indicated in the legend (the number in the symbol key refers to series number in Table 1). It is clear that the criterion $Q_{\text{bar}} \geq 1.1$ formulated by Efstathiou et al. (1982) for indicating stability against bar formation provides a rough guide for our restricted class of simulations, even though it has been shown to fail in more general situations (Athanasoula 2008). Parameters such as minor or major disk orientation, or the residual asphericity of the dark matter halo, appear to be only of secondary importance.

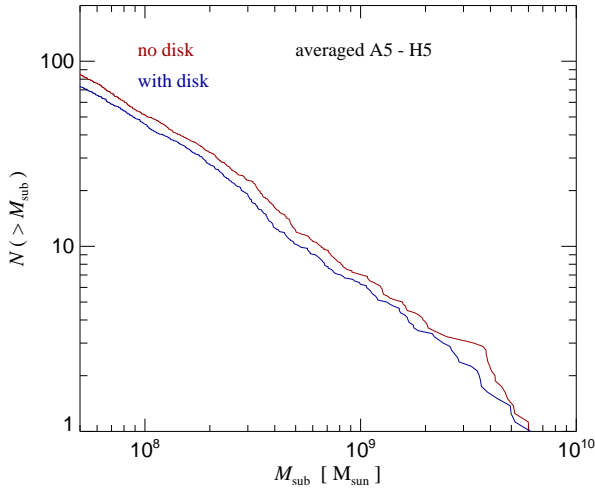


Figure 18. Change of the cumulative abundance of substructures as a function of mass due to presence of a stellar disk. We count all substructures identified by SUBFIND within 200 kpc of the halo centers, and averaged over our 8 Aquarius halos. The “no disk” runs refer to results at $z = 0$ of pure dark matter only runs of the halos where no stellar component is inserted, while the “with disk” results are for our default disk systems of simulation series #1.

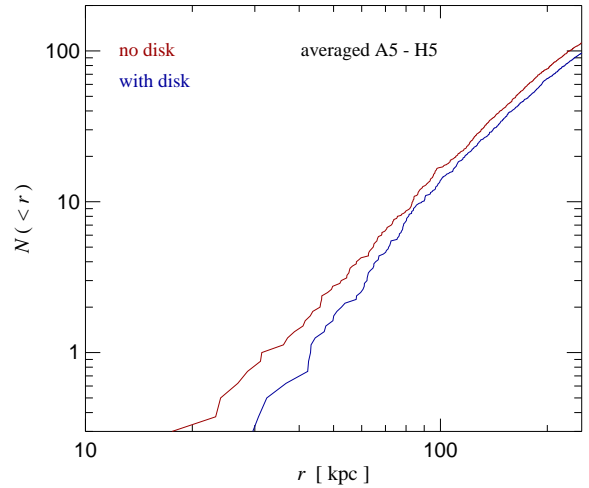


Figure 19. Change of the cumulative abundance of substructure as a function of radius due to presence of a stellar disk. We count all substructures identified by SUBFIND with a mass larger than $6 \times 10^7 M_{\odot}$, and average over our 8 primary galaxy models. The comparison corresponds to that shown in Fig. 18, but considers the radial distribution instead of the mass distribution.

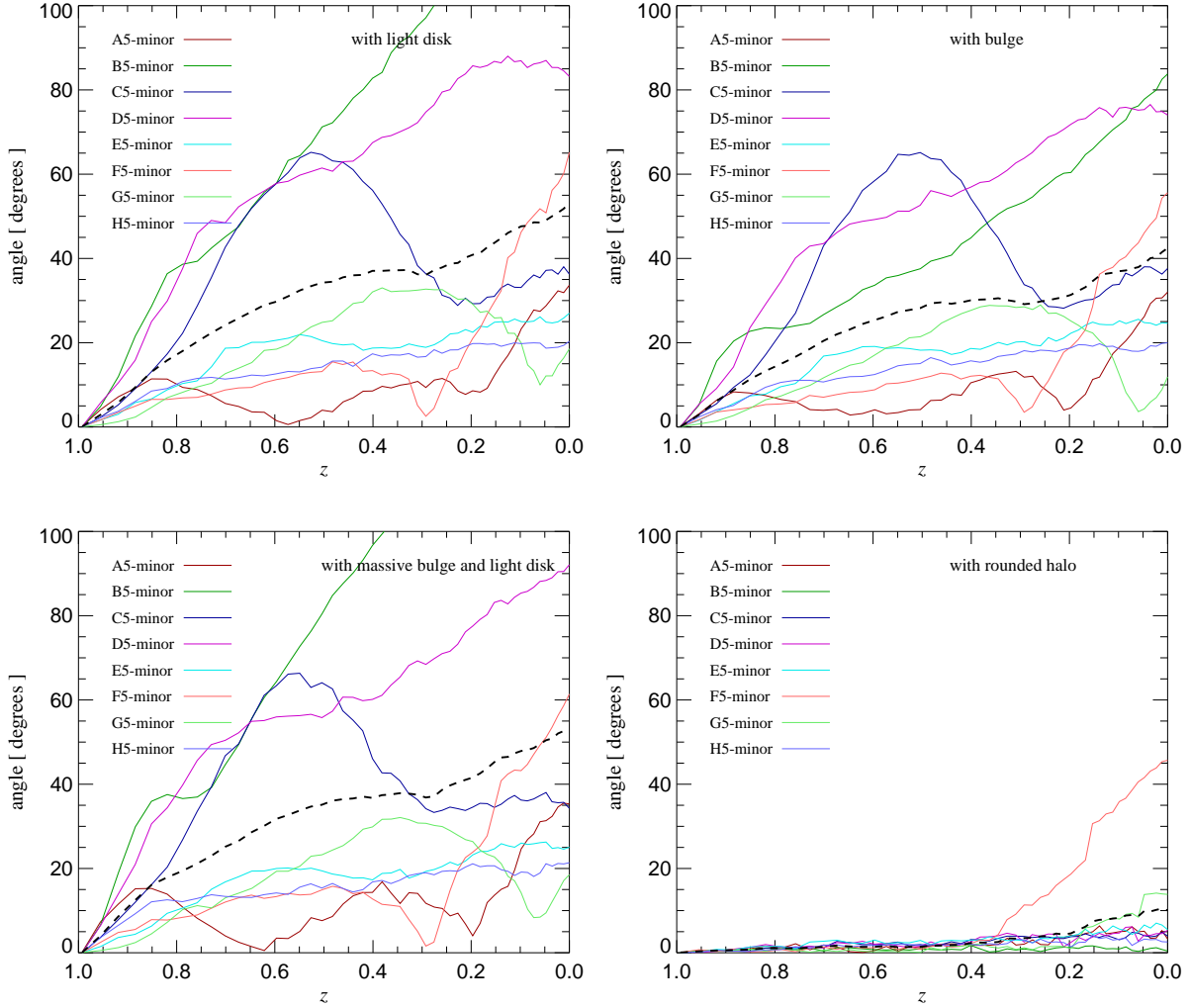


Figure 17. Angle between the current disk spin axis and the initial disk orientation as a function of time, for different types of simulations. The top left panel shows results for our simulation series #4, where a lighter disk is used compared with our default disk runs. The top right panel shows our default disk+bulge models instead (series #3), whereas the bottom left gives the tilt angle evolution for our simulations with massive bulges and a light disk (series #5). Finally the bottom right is for our default pure disk simulations, but this time the dark matter halo has been artificially rounded at $z = 1.3$ when the disk was inserted (series #6). Interestingly, the disk structural properties appear to play only a minor role for the disk tumbling (compare also to Fig. 4). The latter is clearly governed by the dark matter halo and can only be eliminated by substantial rounding that is far stronger than the effects achieved by the halo’s response to the growing baryonic component.

are in good agreement with the analysis of D’Onghia et al. (2010), who carried out orbit integrations for the subhalos found in the dark matter only simulations of Aquarius and estimated their evaporation rate analytically by summing up the impact of gravitational shocks (Ostriker et al. 1972) experienced during disk passages.

In order to explicitly test for the influence of substructures on disk heating and disk stability, we have carried out a series of runs where we varied our “rounding halo” experiment above. Instead of sphericalizing all dark matter particles in the halo at $z = 1.3$, we have done so only for the dark matter particles bound in substructures. Combined, these subhalos amount to a few percent of the mass of the halo, so by redistributing the substructure particles in a spherical fashion, the halo is made smooth without affecting its dynamical equilibrium much. We note however that a large fraction of the substructures found in a halo at low redshift will be accreted at $z < 1.3$; they are unaffected, and so this cleaning of substructure

will only temporarily make the halo smooth. This is seen explicitly in Figure 20, where we show the abundance of substructures as a function of radius at different times, comparing an ordinary disk run with a run where the substructure cleaning has been carried out at $z = 1.3$. While at $z = 1.25$ the inner halo is still largely devoid of subhalos in the cleaned run, in the redshift range $1 < z < 0.85$, the abundance is suppressed on average by a factor of 2, whereas towards $z = 0$ it is down by only $\sim 20\%$.

We now use the subhalo cleaning run to look at differences of the disk heating rates between $z = 1.0$ and $z = 0.85$. At this time, the disks are still largely intact even in the runs that form strong bulges, and here the substructure suppression in the runs with the subhalo cleaning is still substantial and fairly uniform across radius and in time. In Figure 21 we show the difference in the vertical velocity dispersion in the standard runs and the runs with subhalo cleaning. We clearly see evidence for an enhanced heating rate of

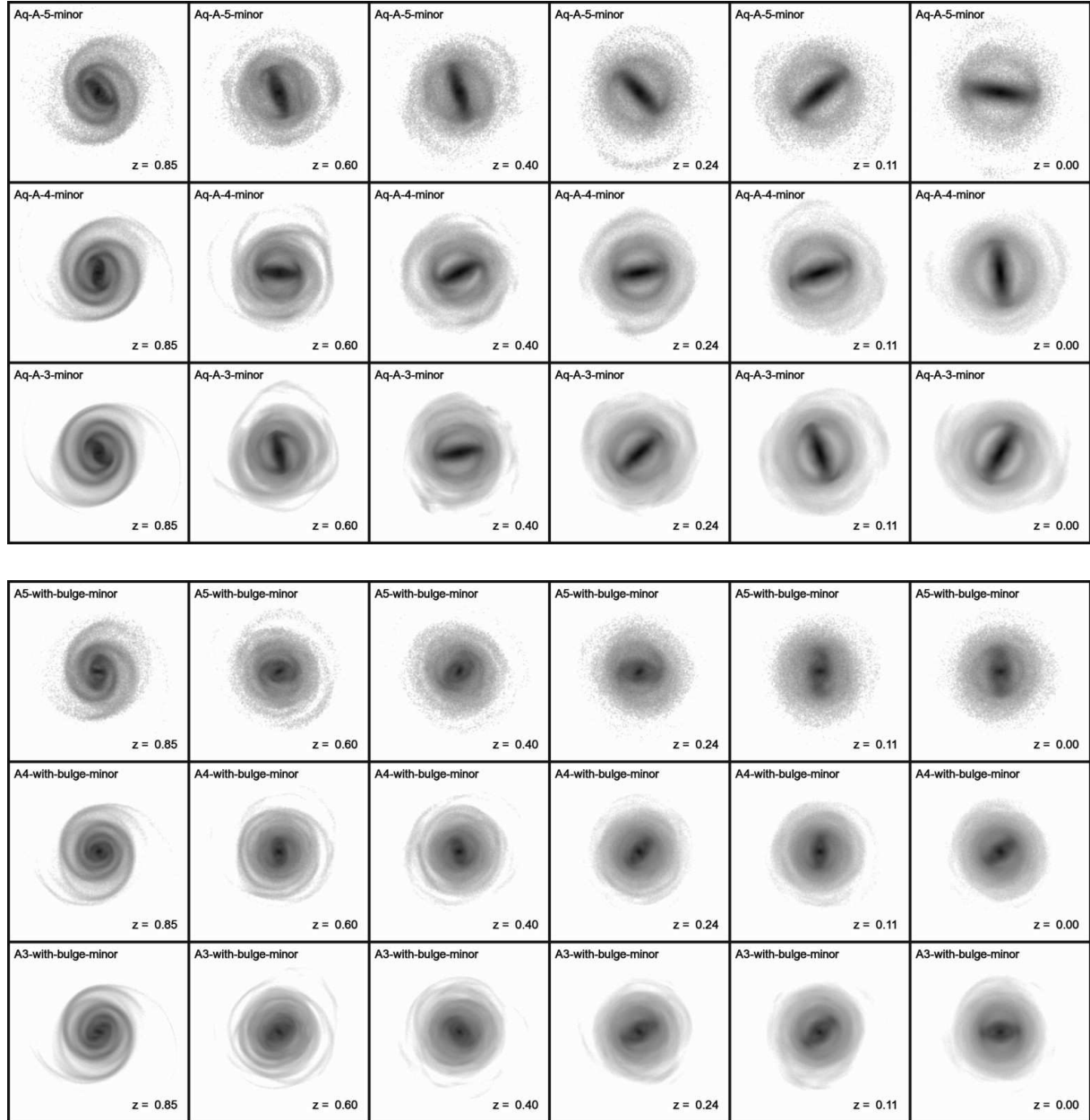


Figure 22. Resolution dependence of disk morphology in our default runs with pure disks (series #1) and disks+bulges (series #3). The top three rows of images compare the face-on projections of the stellar disks at different times of our simulations of A5, A4, and A3 in the runs with pure disks. The corresponding simulations where a third of the stellar mass is moved to a central bulge are shown in the bottom three rows. It is reassuring that the runs agree rather well, apart from the phase angle of the bar.

the disks in their outer parts, amounting to several km s^{-1} over the course of 1 Gyr. However, within two disk scale lengths, there is virtually no detectable difference in the disk heating rate, suggesting that substructure heating is negligible for the bulk of the disk’s stellar mass. It may however play an important role in contributing to flaring of the stellar disk in the outer parts.

7 RESOLUTION DEPENDENCE

So far, all our results have been based on ‘level-5’ Aquarius simulations, with a resolution of 2×10^5 particles in the disk, a dark matter halo resolved by about 10^6 particles, and a gravitational softening

length of 680 pc. Some effects of galactic dynamics can depend strongly on numerical resolution (e.g. Weinberg & Katz 2002), so it is advisable to check the robustness and numerical convergence of our primary results in the relevant regime.

To this end we have repeated our primary A-5 simulations at two higher resolution levels, where the particle number is increased by factors of 8 and 64, respectively, in both the dark matter and stellar components. The gravitational softening lengths are reduced by factors of 2 and 4, respectively. In our highest resolution simulation A-3, this means that the stellar disk is represented with 12.8 million particles, the stellar bulge (if present) with 6.4 million, and the dark matter halo with about 50 million particles.

In Figure 22 we show a visual comparison of the stellar disk

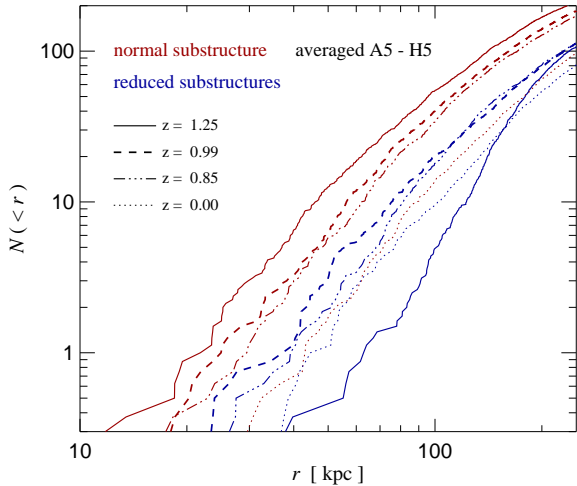


Figure 20. Illustration of the impact of our “substructure cleaning” procedure where at the disk insertion redshift of $z = 1.3$ all particles in bound substructures of the central FOF group are spherically redistributed. The plot shows the cumulative radial abundance of substructures with mass above $6 \times 10^7 M_{\odot}$ at different times, comparing runs where the substructure reduction was carried out with normal simulations where this was not done. At $z = 1.25$, the reduction of subhalos in the inner parts of the target halo is still very strong, but soon the subhalo population is replenished by the accretion of additional mass and substructures. This reduces the substructure reduction effect at late times substantially, but in the range $1.0 < z < 0.85$ it is more or less constant as a function of radius and amounts to a suppression of around a factor of 2.

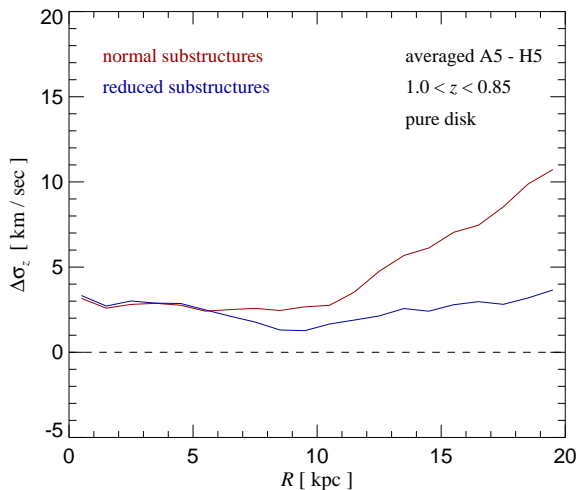


Figure 21. Differential heating of the stellar disk in runs with normal or reduced substructure abundance. We here show radial profiles of the increase of the vertical velocity dispersion of disk stars between times $z = 1$ and $z = 0.85$ in our runs with pure disks. The reference simulations correspond to series #1, while in the comparison runs of series #8 the substructure has been smoothed out at the disk insertion time ($z_{\text{insert}} = 1.3$). In the runs with reduced substructure abundance, we find a substantially reduced heating rate in the outer parts of the disk, whereas in the inner parts within two disk scale lengths no difference is detected.

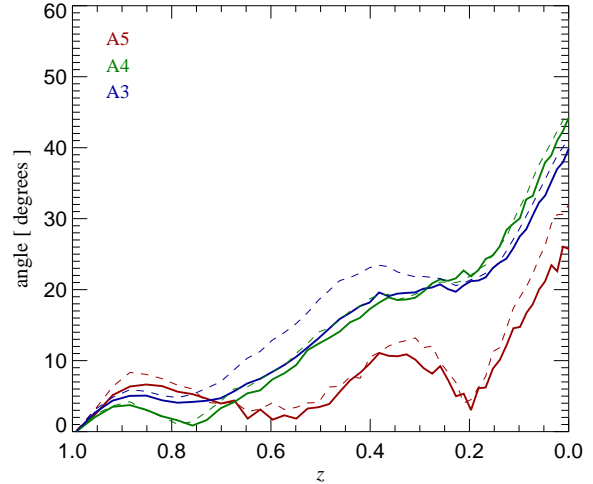


Figure 23. Disk tilt angle measured for simulations at different numerical resolutions, ranging from Aquarius level-5 to level-3. Two types of runs are shown, the A-halo with a pure disk (solid lines, from series #1), and the A-halo with a disk+bulge (dashed lines, from series #3). The tilt angles of the disks do not line up quantitatively in detail for the different resolutions, but the evolution qualitatively still agrees reasonably well, without any indication of systematic trends with resolution. The tilt angle evolution for a given resolution is almost identical for runs with or without a bulge, showing that it is governed almost exclusively by the dark matter halo, so that the difference we find between A3, A4, and A5 likely originate in small differences of the dynamical states of their dark matter halos when the disk is inserted.

evolution seen in the three resolution levels. The top three rows compare pure disk models at the resolution levels 5, 4, and 3, whereas the bottom three rows give the same comparison for our standard models with bulges. Overall, the disk morphologies are very similar in both resolution sequences. The position angles of the bar motion do not line up exactly, but such phase differences are to be expected. However, the overall morphological evolution is clearly very similar, which suggests good convergence of the structural evolution of the galaxies.

More quantitatively, we show in Figure 23 a convergence study of the tilt angle evolution in the two resolution sequences. Especially the two high resolution runs line up remarkably well. The lower resolution run shows a small offset in its evolution in comparison, but since there is no systematic trend with resolution we interpret this small difference in angle as a chance effect. Other quantities we examined are similarly stable with respect to resolution. We hence believe that already the level-5 resolution provides robust results for the quantities studied in this work.

8 DISCUSSION AND CONCLUSIONS

In this study, we have analyzed the stability of disk galaxies inserted into high-resolution zoom-simulations of the formation of Milky Way-sized dark matter halos, with initial conditions taken from the Aquarius project. We have refined a methodology previously used by DeBuhr et al. (2012), most notably by employing a more sophisticated approach to determine the initial velocity distribution of the star particles. For the latter we made use of the iterative method realized in the GALIC code (Yurin & Springel 2014), which is capable of computing high-quality stationary solutions in general dark matter halos. For the dark matter potential, we directly

used the distribution of dark matter particles found in the Aquarius halos, without using any approximations besides imposing axisymmetry on the force field.

Using this improved methodology, we have extended the analysis of the Aquarius halos to a larger halo sample (using eight systems, A to H), and to structural variants that also include systems with central bulges. We have also investigated a number of toy simulations where the dark matter halos were artificially rounded or dark matter substructures were erased, in order to highlight the impact of residual triaxiality and of substructures on the dynamical evolution of the disks.

Our main findings can be summarized as follows:

(i) The presence/absence of a stellar bulge, as well as the presence/absence of a stellar bar, do not significantly affect the tumbling of disk galaxies. The turning motion of disks appears to be primarily driven by the triaxiality of the halo and its figure rotation; in rare cases encounters with massive substructures can also initiate substantial disk tilt.

(ii) Disks initially oriented along the dark matter halo's minor axis show on average better directional stability than disks oriented along the major axis.

(iii) We predict that an average tumbling angle of about 40 degrees over 7.6 Gyr between $z = 1$ and $z = 0$ should be quite typical for disk galaxies, corresponding to 5 – 6 degrees per Gyr. Importantly, thin disks can survive such tumbling rates in a largely unaffected way.

(iv) There is a significant depletion of dark matter substructures due to the presence of a massive disk. If part of the disk mass is put into a bulge instead, the effect is very slightly reduced, suggesting that gravitational shocking at the disk is indeed more important than the enhancement of the central core density and the associated increase of pericenter at the halo cusp.

(v) Dark matter substructure can significantly contribute to disk heating in the outer parts of disks, while this appears largely negligible in the inner regions within $\simeq 2$ disk scale lengths.

(vi) Our quantitative numerical results are unaffected by numerical resolution, as evidence by our resolution tests that cover a factor of 64 in mass resolution, and a factor of 4 in gravitational softening length.

Overall, our results suggest that the survival of thin stellar disks is in principle not a problem in CDM halos. In particular, the triaxiality and high substructure abundance in CDM halos do not preclude the survival of thin stellar disks, even though we would expect them to tumble slowly with time. What is arguably more difficult to understand is how massive, cold stellar disks can survive strong bar formation. Cuspy cold dark matter halos actually help here, whereas the low central dark matter densities often inferred observationally for the inner parts of galaxies (even for the Milky Way, see Bovy & Rix 2013) make it challenging to understand how such observed systems manage to sport only a small or no bar. This remains an interesting topic for further study.

The results obtained here demonstrate the power of our techniques to introduce stellar systems into cosmologically consistent, growing dark matter halos. This facilitates research in galactic dynamics at very high resolution within a realistic and complex cosmological environment, something that promises to be a worthwhile avenue for future work.

ACKNOWLEDGMENTS

We thank the anonymous referee for constructive criticism and valuable suggestions that helped to improve the paper. D.Y. acknowledges support by the DFG Research Centre SFB-881 'The Milky Way System' through project A6. This work has also been supported by the European Research Council under ERC-StG grant EXAGAL-308037 and by the Klaus Tschira Foundation.

REFERENCES

- Agertz O., Teyssier R., Moore B., 2011, *MNRAS*, 410, 1391
 Allgood B., Flores R. A., Primack J. R., Kravtsov A. V., Wechsler R. H., Faltenbacher A., Bullock J. S., 2006, *MNRAS*, 367, 1781
 Athanassoula E., 2002, *ApJ*, 569, L83
 Athanassoula E., 2008, *MNRAS*, 390, L69
 Athanassoula E., Misiriotis A., 2002, *MNRAS*, 330, 35
 Aumer M., White S. D. M., 2013, *MNRAS*, 428, 1055
 Aumer M., White S. D. M., Naab T., 2014, *MNRAS*, 441, 3679
 Aumer M., White S. D. M., Naab T., Scannapieco C., 2013, *MNRAS*, 434, 3142
 Berentzen I., Shlosman I., 2006, *ApJ*, 648, 807
 Berentzen I., Shlosman I., Jogee S., 2006, *ApJ*, 637, 582
 Binney J. et al., 2014, *MNRAS*, 439, 1231
 Binney J., Tremaine S., 1987, *Galactic dynamics*. Princeton, NJ, Princeton University Press
 Bovy J., Rix H.-W., 2013, *ApJ*, 779, 115
 Büdenbender A., van de Ven G., Watkins L. L., 2014, *ArXiv e-prints*, 1407.4808
 Debattista V. P., Mayer L., Carollo C. M., Moore B., Wadsley J., Quinn T., 2006, *ApJ*, 645, 209
 Debattista V. P., Roškar R., Valluri M., Quinn T., Moore B., Wadsley J., 2013, *MNRAS*, 434, 2971
 DeBuhr J., Ma C.-P., White S. D. M., 2012, *MNRAS*, 426, 983
 Diemand J., Moore B., Stadel J., 2004, *MNRAS*, 352, 535
 D'Onghia E., Springel V., Hernquist L., Keres D., 2010, *ApJ*, 709, 1138
 Efstathiou G., Lake G., Negroponte J., 1982, *MNRAS*, 199, 1069
 Frenk C. S., White S. D. M., Davis M., Efstathiou G., 1988, *ApJ*, 327, 507
 Gauthier J.-R., Dubinski J., Widrow L. M., 2006, *ApJ*, 653, 1180
 Ghigna S., Moore B., Governato F., Lake G., Quinn T., Stadel J., 1998, *MNRAS*, 300, 146
 Governato F. et al., 2010, *Nature*, 463, 203
 Guedes J., Callegari S., Madau P., Mayer L., 2011, *ApJ*, 742, 76
 Guo Q., White S., Li C., Boylan-Kolchin M., 2010, *MNRAS*, 404, 1111
 Hayashi E., Navarro J. F., Springel V., 2007, *MNRAS*, 377, 50
 Heller C. H., Shlosman I., Athanassoula E., 2007, *ApJ*, 671, 226
 Hernquist L., 1990, *ApJ*, 356, 359
 Kazantzidis S., Bullock J. S., Zentner A. R., Kravtsov A. V., Moustakas L. A., 2008, *ApJ*, 688, 254
 Kazantzidis S., Zentner A. R., Kravtsov A. V., Bullock J. S., Debattista V. P., 2009, *ApJ*, 700, 1896
 Landau L. D., Lifshitz E. M., 1969, *Mechanics*. Oxford: Pergamon Press
 Machado R. E. G., Athanassoula E., 2010, *MNRAS*, 406, 2386
 Marinacci F., Pakmor R., Springel V., 2014a, *MNRAS*, 437, 1750
 Marinacci F., Pakmor R., Springel V., Simpson C. M., 2014b, *MNRAS*, 442, 3745
 Martinez-Valpuesta I., Shlosman I., Heller C., 2006, *ApJ*, 637, 214

- Moore B., Ghigna S., Governato F., Lake G., Quinn T., Stadel J., Tozzi P., 1999, *ApJL*, 524, L19
- Moster B. P., Somerville R. S., Maulbetsch C., van den Bosch F. C., Macciò A. V., Naab T., Oser L., 2010, *ApJ*, 710, 903
- Navarro J. F. et al., 2010, *MNRAS*, 402, 21
- Okamoto T., Isoe M., Habe A., 2015, *PASJ*
- Ostriker J. P., Spitzer, Jr. L., Chevalier R. A., 1972, *ApJL*, 176, L51
- Pakmor R., Marinacci F., Springel V., 2014, *ApJL*, 783, L20
- Purcell C. W., Kazantzidis S., Bullock J. S., 2009, *ApJL*, 694, L98
- Read J. I., Lake G., Agertz O., Debattista V. P., 2008, *MNRAS*, 389, 1041
- Romano-Díaz E., Shlosman I., Heller C., Hoffman Y., 2008, *ApJL*, 687, L13
- Scannapieco C. et al., 2012, *MNRAS*, 423, 1726
- Scannapieco C., White S. D. M., Springel V., Tissera P. B., 2009, *MNRAS*, 396, 696
- Sellwood J. A., Nelson R. W., Tremaine S., 1998, *ApJ*, 506, 590
- Shen S., Mo H. J., White S. D. M., Blanton M. R., Kauffmann G., Voges W., Brinkmann J., Csabai I., 2003, *MNRAS*, 343, 978
- Siebert A. et al., 2008, *MNRAS*, 391, 793
- Springel V., 2005, *MNRAS*, 364, 1105
- Springel V., 2010, *MNRAS*, 401, 791
- Springel V. et al., 2008a, *MNRAS*, 391, 1685
- Springel V. et al., 2008b, *Nature*, 456, 73
- Springel V. et al., 2005, *Nature*, 435, 629
- Springel V., White S. D. M., Tormen G., Kauffmann G., 2001, *MNRAS*, 328, 726
- Stinson G. S. et al., 2013, *MNRAS*, 436, 625
- Toomre A., 1964, *ApJ*, 139, 1217
- Velazquez H., White S. D. M., 1999, *MNRAS*, 304, 254
- Walker I. R., Mihos J. C., Hernquist L., 1996, *ApJ*, 460, 121
- Weinberg M. D., Katz N., 2002, *ApJ*, 580, 627
- Xu D. D. et al., 2009, *MNRAS*, 398, 1235
- Yurin D., Springel V., 2014, *MNRAS*, 444, 62
- Zhang Y., Yang X., Wang H., Wang L., Luo W., Mo H. J., van den Bosch F. C., 2015, *ApJ*, 798, 17